Review | Open Access

Energy Materials

Chen *et al. Energy Mater.* **2026**, *6*, 600124 **DOI:**10.20517/energymater.2026.154

Syngas to higher alcohols: a review of catalyst design and progress

Gaofeng Chen[1,2,*], Xinzhu Mei[1], Zhiwei Wang[1,2,*], Na Guo[1,2], Qun Wang[1,2], Tian Wang[1], Xue Song[1]

Keywords:
Dual carbon goal, higher alcohol synthesis, syngas, modified Fischer-Tropsch catalysts, Cu-Co catalyst, Cu-Fe catalyst

Citation: Chen, G.; Mei, X.; Wang, Z.; Guo, N.; Wang, Q.; Wang, T.; Song, X. Syngas to higher alcohols: a review of catalyst design and progress. *Energy Mater.* **2026**, *6*, 600124. https://dx.doi.org/10.20517/energymater.2026.154

Received: 4 Jun 2026
First Decision: 17 Jul 2026
Revised: 30 Aug 2026
Accepted: 7 Sep 2026
Published: 22 Sep 2026

Academic Editor:
Yuhui Chen
Copy Editor:
Ping Zhang
Production Editor:
Ping Zhang

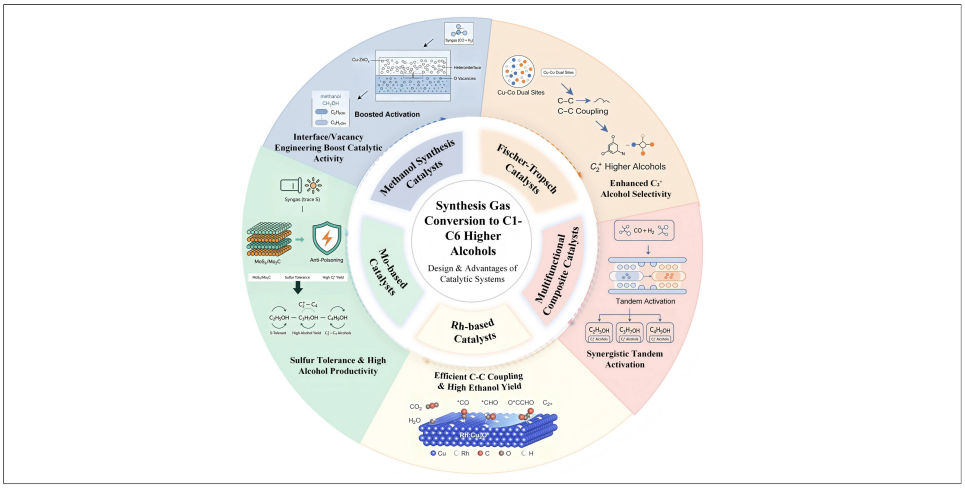

Abstract

Syngas-derived higher alcohols ($C_{2+}OH$) are vital clean fuels under dual-carbon targets, yet inherent catalytic bottlenecks hinder industrialization. This review systematically correlates core defects across five mainstream catalyst families with targeted modification strategies and structure-selectivity rules. Cu-Co catalysts exhibit overly broad product distribution and phase segregation; La/Mn doping and plasma activation accelerate C-C coupling. Cu-Fe catalysts sinter easily and undergo phase separation; Mg/K/Ce doping and carrier tuning reinforce bimetallic interfacial synergy. Modified Cu methanol catalysts lack stable active sites; particle size control, pH adjustment, and ammonia evaporation enrich Cu-ZnO_x interfaces. Mo catalysts resist sulfur and carbon deposition but require harsh reaction conditions; K/La doping and porous carbon carriers improve long-chain alcohol selectivity. Rh catalysts exhibit excellent $C_{2+}OH$ selectivity but incur high noble-metal costs; single-atom immobilization reduces Rh consumption. Multifunctional tandem catalysts balance activity and selectivity via matched dual active sites. This study establishes a "bottleneck-modification" matching system, offering theoretical support for low-cost high-performance catalysts and industrial syngas-to-higher-alcohol technology.

[1]School of Environmental Engineering, Henan University of Technology, Zhengzhou 450001, Henan, China.
[2]Institute for Carbon Neutrality, Henan University of Technology, Zhengzhou 450001, Henan, China.

***Correspondence to:** Dr. Gaofeng Chen, Prof. Zhiwei Wang, School of Environmental Engineering, Henan University of Technology, Zhengzhou 450001, Henan, China. E-mail: gaofengchen@haut.edu.cn; zw.wang@haut.edu.cn

INTRODUCTION

Against the backdrop of the low-carbon energy transition, technologies for efficient conversion and utilization of carbon resources are vital to mitigate reliance on fossil fuels and reduce carbon emissions[1-7]. Syngas can be produced from diverse feedstocks, including coal, biomass, and CO_2, owing to its feedstock flexibility and mature industrial processes, making it a fundamentally important reaction platform with strong industrialization potential in chemical and energy conversion fields[8-11]. Direct catalytic conversion of CO_2 to methanol and higher alcohols is a pivotal technology for utilizing greenhouse gases to produce high-value chemicals and fuels. Taking alcohol synthesis via CO_2 hydrogenation as an example, the overall reaction process consists of two major branches: methanol synthesis and higher alcohol synthesis, accompanied by multiple mutually competitive reaction pathways, as illustrated in Figure 1A[12]. The left side depicts the reaction pathways for methanol synthesis, encompassing four distinct channels: the $HCOO^*$ pathway, r-$HCOO^*$ pathway, RWGS+CO-Hydro pathway, and trans-$COOH^*$ pathway. The right side illustrates the synthetic routes for higher alcohols, covering three prevailing mechanisms: the CO-mediated mechanism, formate-mediated mechanism, and methanol-mediated mechanism. Furthermore, the figure uses lines of different colors to distinguish C-H, C-O, C-C, and O-H bond cleavage and formation, intuitively delineating the evolution, transformation, and competitive relationships among diverse adsorbed intermediates. First, CO_2 is activated to produce C_1 intermediates including $HCOO^*$, $COOH^*$, CO^*, and CH_x^*. Second, C-C coupling occurs between CO^* and CH_x^* to generate C_{2+} oxygenated intermediates such as acetic acid, propionic acid, and butyric acid. Finally, these C_{2+} oxygenated intermediates undergo hydrogenation to yield C_{2+} alcohols[13]. Higher alcohols are compatible with existing industrial and transportation infrastructure and offer the dual benefits of energy substitution and carbon resource recycling. Compared with conventional routes such as biological fermentation and petroleum-based synthesis, syngas-to-higher-alcohols technology features a simplified process, high energy efficiency, environmental friendliness, and flexible feedstock supply, making it a promising candidate for large-scale production of higher alcohols[14-16].

Although the synthesis of higher alcohols from syngas is thermodynamically feasible, formidable technical bottlenecks remain for practical implementation. The reaction system involves an extremely intricate reaction network that requires the synergy of dual active sites responsible for CO dissociation and CO insertion, respectively[16]. Precise matching of active sites and fine-tuning of product selectivity remain challenging. Undesired side reactions readily occur, leading to low yields of target products and poor economic viability, thereby severely hindering the large-scale deployment of this technology.

Accordingly, developing catalysts with high activity, superior selectivity, and excellent stability; elucidating precise regulation strategies for dual active sites; optimizing reaction pathways; and suppressing side reactions are critical to overcoming industrialization barriers in syngas conversion to higher alcohols. On this basis, this study focuses on the optimized design and catalytic performance of catalysts for syngas-to-higher-alcohols synthesis. The structure-activity relationship among catalyst structure, active sites, and catalytic performance is systematically investigated to provide theoretical guidance and technical references for advancing the industrialization of efficient higher alcohol synthesis[13,17].

CO_2 TO HIGHER ALCOHOLS

Massive emissions from fossil fuels increase demand for CO_2 resource utilization. The cleavage energy of the C=O bond in CO_2 reaches up to 1.9 eV, imposing substantial challenges for CO_2 activation. The reverse water-gas shift (RWGS) reaction can be coupled with multiple reactions, including CO_2 hydrogenation[18], Fischer-Tropsch synthesis[19], and higher alcohol synthesis from syngas[20], forming a complex competitive reaction network. Such coupling reshapes the design logic for catalytic materials considering electronic effects, interfacial interactions, mass transfer, and active sites. Regulating multivalent active sites and

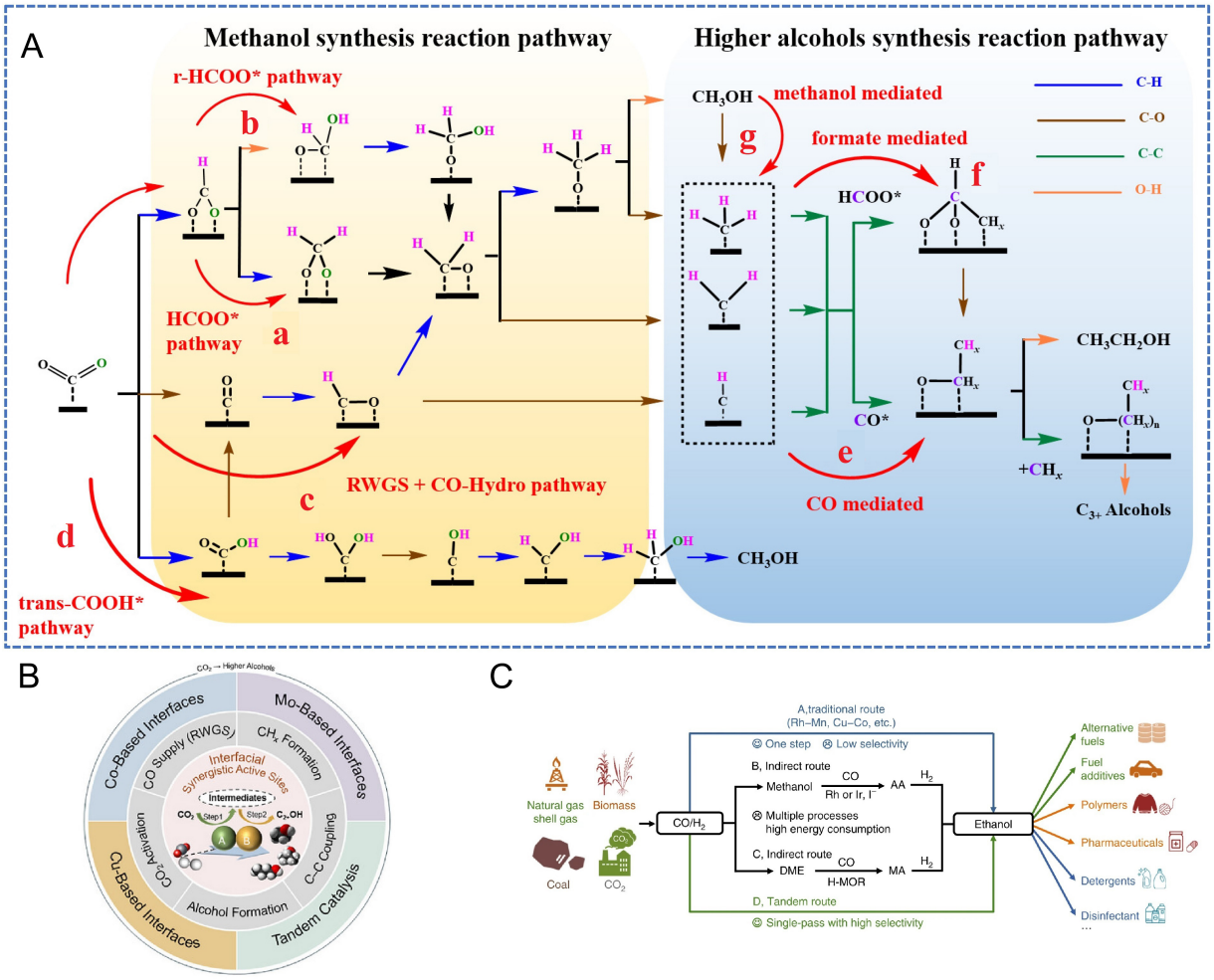

Figure 1. (A) Various reaction pathways of CO_2 hydrogenation to alcohols. (a) HCOO* pathway; (b) r-HCOO* pathway; (c) RWGS + CO-Hydro pathway; (d) trans-COOH* pathway; (e) CO mediated pathway; (f) formate mediated pathway; (g) methanol mediated pathway. Blue line, C-H bond breaking or formation; brown line, C-O bond breaking or formation; green line, C-C bond coupling; orange line, O-H bond breaking or formation. (A) is reprinted with permission from Ref.[12], Copyright © 2024 MDPI; (B) Interfacial active sites play a central role in CO_2 hydrogenation to higher alcohols by promoting CO_2 activation, C-C coupling, and oxygenate stabilization. (B) is reprinted with permission from Ref.[33], Copyright © 2026 John Wiley and Sons; (C) Direct and indirect routes for STE conversion. (C) is reprinted with permission from Ref.[36], Copyright © 2020 Springer Nature. RWGS: Reverse water-gas shift; STE: syngas-to-ethanol; H-MOR: hydrogen-form mordenite.

defective vacancies is the core strategy for efficient CO_2 activation. B-site doping of Ru/V in perovskites reduces the formation energy of oxygen vacancies and strengthens orbital interactions with CO_2[21,22]. For CuV_xS sulfides, *in situ* formation of Cu-S-V linkages stabilizes Cu^+/Cu^{2+} species, prevents excessive reduction of metallic sites, and facilitates the directional generation of methanol intermediates during thermal CO_2 hydrogenation[23]. In C_{2+} alcohol synthesis from syngas, mismatched sites for CO activation and carbon-chain propagation, along with a broad product distribution, represent a common bottleneck for Cu-Co, Cu-Fe, Mo-based, and Rh-based catalysts[17].

The RWGS reaction exhibits dual characteristics: it supplies CO in the forward direction yet generates CO_2 as a byproduct, which drastically lowers carbon utilization efficiency[24]. Two representative modulation strategies are exemplified as follows. First, confining Cu within CeO_2 to construct strong metal-support interaction (SMSI) interfaces optimizes the RWGS reaction kinetics[25]. Second, hydrophobic modification of Fe catalysts creates unidirectional water channels that isolate water molecules from active sites, suppressing

side reactions; accordingly, CO_2 selectivity can be reduced to 14.3%[26]. Alcohol synthesis from syngas requires balanced activity of the forward and reverse water-gas shift reactions. Fe-based catalysts tend to produce CO_2 as a byproduct, while monometallic Cu catalysts lack sites for carbon chain growth and cannot extend carbon chains using CO derived from RWGS. Doping Mo sulfides and carbides with K or Ni enables precise tuning of reaction compatibility, rendering such catalysts suitable for long-chain alcohol synthesis.

Distinct stabilization strategies are required under varied operating conditions. Under reducing atmospheres, Fe-Ru and Fe-Co alloy nanoparticles at the B site can be exsolved *in situ* from the parent lattice. Strong pinning interfaces between nanoparticles and substrates suppress particle migration and agglomeration in conventional impregnated catalysts. These catalysts operate stably at temperatures up to 800 °C with high activity and no carbon deposition over long periods[27]. Modification with composite supports (e.g., oxygen-defect-rich composite oxides and coupled hollow zeolites) expands triple-phase boundaries (TPBs), accelerates bulk O_2 transport, and significantly promotes the regeneration of active oxygen vacancies, addressing sluggish reaction kinetics at high space velocities[28,29]. For thermal CO_2 hydrogenation systems, heterointerface engineering, *in situ* construction of heteroatomic linkages, and defect modulation work synergistically. The primary design target is to dynamically maintain multivalent active sites, inhibit deep reduction of active metals and leaching of sulfur/oxygen species, ensure exclusive hydrogenation pathways for intermediates during long-term operation, and achieve high selectivity for high-value C1 products such as methanol[23].

Considering multiple constraints covering CO_2 activation, RWGS coupling and synergy, and resource conversion under diverse conditions, three novel core requirements for catalyst design have been established. First, precise modulation of electronic structures. Metal doping, heterointerfaces, heteroatomic bonding, and oxygen vacancy engineering are adopted to construct synergistic multivalent active sites that balance CO_2 adsorption strength with the desorption/hydrogenation kinetics of $^*CO$ and oxygen-containing intermediates. Second, enhanced interfacial and structural stability. Strategies including *in situ* exsolution, confinement encapsulation, SMSI construction, and hydrophobic modification are developed to address four major deactivation pathways: high-temperature sintering, carbon deposition, water-induced side reactions, and reduction/leaching of active phases. Third, multiscale coordinated mass transfer design. Integrating porous hollow architectures, oxygen-vacancy-rich supports with high lattice-oxygen mobility, and hydrophobic pore-channel regulation simultaneously optimizes gas diffusion, lattice-oxygen transport, and unidirectional water transport, reconciling intrinsic catalytic activity with macroscopic reaction flux.

CATALYSTS FAMILIES

The evolution of catalysts has been driven by shifting energy demands and technological breakthroughs. The field was pioneered in 1902 with the discovery that nickel-based heterogeneous catalysts could facilitate the reduction of CO to methane. Between 1913 and 1925, a series of catalysts, including alkali-activated cobalt/osmium oxides, alkali-modified iron filings, and iron-zinc oxides, were developed, marking a significant transition in higher hydrocarbon synthesis from high-pressure to atmospheric-pressure conditions. By the 1940s, cobalt scarcity shifted the focus to alkali-modified iron-based catalysts, which became mainstream because of their cost-effectiveness, superior stability, and flexible product distribution. The energy crisis of the 1970s subsequently accelerated the exploration of homogeneous catalysts, where metal carbonyl clusters and rhodium-based systems demonstrated exceptional selectivity. Concurrently, the emergence of specialized catalysts, such as ZSM-5 zeolites, Fe-Ti-Zn-K mixed oxides, and manganese-based systems, enabled pivotal advancements like methanol-to-gasoline conversion and the targeted synthesis of light olefins[30,31]. The catalytic conversion of syngas represents a crucial pathway for producing higher alcohols, leveraging both renewable and non-renewable carbon resources[32]. As illustrated in Figure 1B, catalytic systems for CO_2 hydrogenation to higher alcohols can be broadly categorized into four classes[33].

Extensive studies indicate that, compared with biomass fermentation and petroleum refining, syngas-to-ethanol (STE) offers distinct advantages in environmental sustainability and economic viability[34,35]. Figure 1C summarizes four technical routes for ethanol synthesis from syngas[36]. Route a refers to the direct synthesis pathway employing a single catalyst, yet it suffers from low ethanol selectivity. Routes b and c correspond to multi-step indirect processes that use methanol and dimethyl ether as intermediates, respectively; these routes require multiple sets of reaction units and incur high energy consumption throughout the process. Route d represents the newly developed triple-tandem catalytic process, which achieves high-selectivity one-pass ethanol production from syngas in a single reactor, circumvents the intrinsic limitations of conventional routes, and enables the targeted synthesis of low-carbon alcohols from syngas.

Modified Fischer-Tropsch catalyst system

Fischer-Tropsch synthesis (FTS) is a pivotal technology for the conversion of syngas (CO/H_2) into hydrocarbons. Pioneered by German scientists Fischer and Tropsch in 1923, the first fixed-bed FTS plant was commissioned in 1935. While early FTS processes relied predominantly on Fe-based catalysts, researchers have since developed other catalytic systems. These include Co-based catalysts, known for their high selectivity toward long-chain hydrocarbons; Ru-based catalysts, distinguished by their superior catalytic activity; and Mo-based catalysts, which exhibit notable resistance to sulfur poisoning[37-39].

Pristine unmodified transition metal nanoparticles suffer from significant drawbacks, including severe particle agglomeration and sintering, as well as facile coverage of active sites by carbon deposits. Furthermore, their uniform electronic and geometric configurations impede precise regulation of carbon chain propagation, resulting in low CO conversion, poor selectivity toward target products, and abundant byproducts during FTS. These limitations render these catalysts incapable of meeting the requirements for high-efficiency, oriented catalysis, highlighting the critical need for catalyst modification and optimization[40,41]. Current modification strategies center on tuning the catalyst microstructures. Specifically, metal doping and crystal phase engineering modulate the electronic and lattice structures of nanoparticles, while support confinement and surface functionalization immobilize active nanoparticles and optimize particle size and dispersion. Together, these approaches improve catalytic performance and boost FTS activity and selectivity toward desired products[42,43].

Figure 2A provides a comparative overview of two typical CO reduction pathways. Electrochemical CO reduction over Cu catalysts under ambient conditions proceeds via direct coupling of two adsorbed CO species; this CO-CO coupling acts as the rate-determining step, with a high energy barrier dominating the production of short-chain C_2 products[44]. Conversely, thermocatalytic Fischer-Tropsch synthesis generates adsorbed hydrogen via H_2 dissociation, followed by C-O bond cleavage of CO to form CH_x intermediates[45]. Subsequent low-barrier CH_x coupling enables continuous carbon chain propagation to afford long-chain hydrocarbons, yet high temperatures are required to facilitate CO dissociation. Fundamentally, this process converts syngas over transition-metal catalysts (e.g., Fe, Co, Ni, Ru) [Figure 2B] through a multifaceted sequence of adsorption, dissociation, intermediate transformation, and product formation[46]. This yields hydrocarbons (alkanes, alkenes) and oxygenates (alcohols, aldehydes), alongside byproducts such as H_2O and CO_2. The reaction is inherently synergistic, involving surface-catalyzed polymerization and hydrogenation. Furthermore, the pivotal step in FTS is carbon-carbon bond formation, which critically depends on well-dispersed transition metal nanoparticle catalysts. Both catalytic activity and product selectivity are intrinsically linked to the electronic and geometric structures of the nanoparticles, which are governed by key parameters such as particle size, morphology, and crystal phase structure[46-48].

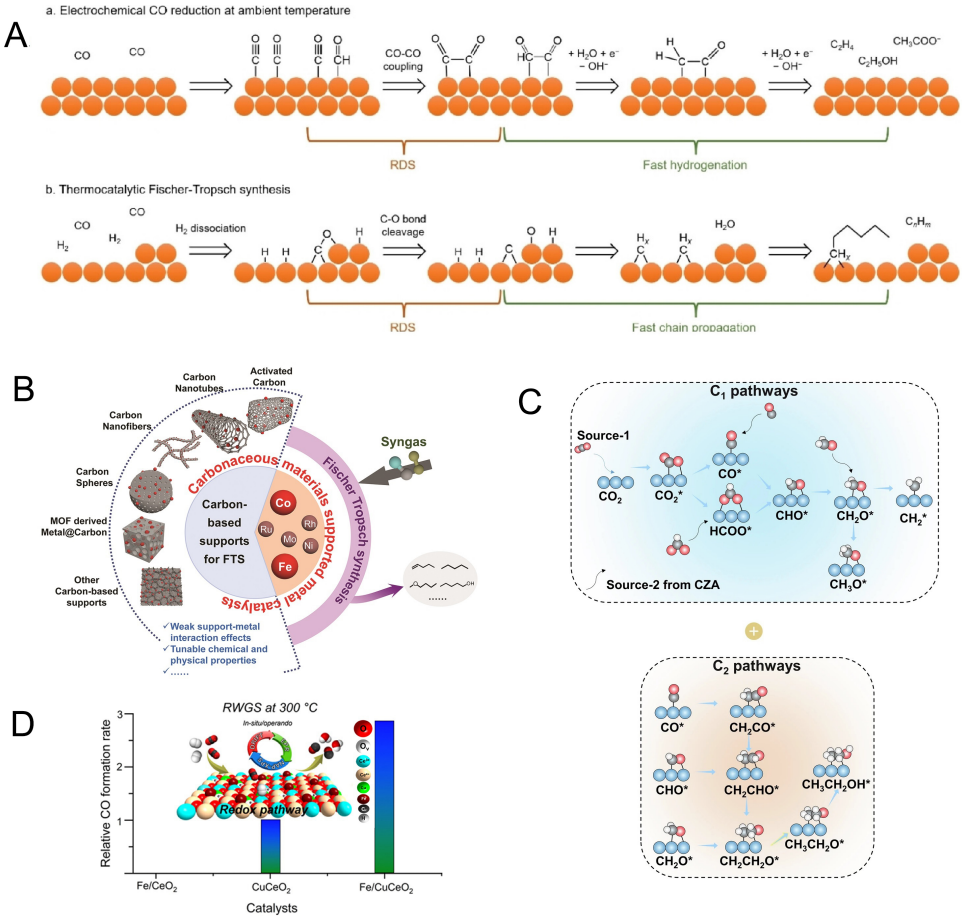

Figure 2. (A) Schematics of different COR pathways. (a) Electrochemical CO reduction at ambient temperature. (b) Thermocatalytic FTS. (A) is reprinted with permission from Ref.[44], Copyright © 2025 John Wiley and Sons; (B) Carbonaceous materials supported metal catalysts for FTS. (B) is reprinted with permission from Ref.[46], Copyright © 2021 Royal Society of Chemistry; (C) Reaction mechanism for C_{2+}OH synthesis on the FeCo&CZA catalyst. The optimal reaction pathway for ethanol synthesis on $(Fe_{3/4}Co_{1/4})_5C_2(510)$ surface. Color: C: Gray, H: White, O: Red. (C) is reprinted with permission from Ref.[52], Copyright © 2025 Springer Nature; (D) Overview of the Redox Mechanism and Surface Structure Changes on the Fe/$CuCeO_2$ Catalyst during the RWGS Reaction. (D) is reprinted with permission from Ref.[54], Copyright © 2024 American Chemical Society. RWGS: Reverse water-gas shift; FTS: Fischer-Tropsch synthesis; CZA: CuZnAl.

Fe-based catalysts exhibit dual functionality in both RWGS and FTS, achieving C_{5+} hydrocarbon selectivity exceeding 50%[49]. However, promoters are essential for accelerating carbide formation. Conversely, Co/Ru-based catalysts are characterized by high methane selectivity (> 90%) but are constrained by the thermodynamic limitations of the RWGS reaction, which limit CO partial pressure and necessitate advanced techniques, such as membrane reactors, to enhance CO coverage[50,51]. Wang *et al.*[52] doped cobalt into iron to fabricate a tandem FeCo alloy carbide/CuZnAl catalyst for CO_2 hydrogenation to C_{2+} alcohols. The CuZnAl (CZA) component activates CO_2 and produces abundant CH_2O^* oxygen-containing intermediates via the reverse water-gas shift reaction, which subsequently spill over onto the FeCo active sites. Co incorporation generates $(Fe_{3/4}Co_{1/4})_5C_2$ alloy carbide and modulates its electronic structure to moderate oxygen affinity, thereby eliminating the drawbacks of monometallic iron carbide, including susceptibility to water oxidation and excessive cleavage of C-O bonds that favors hydrocarbon formation. Two distinct active sites on the alloy carbide surface simultaneously supply CH_2O^* and CH_2^* species, which undergo C-C coupling with a low 0.52 eV barrier. The coupled intermediates are further hydrogenated to preferentially yield ethanol. This catalytic system achieves high CO_2 conversion, superior C_{2+} alcohol selectivity, and outstanding long-term stability [Figure 2C][52]. The resulting FTS products can be further refined into a diverse array of high-value chemicals, including light olefins, gasoline, diesel, waxes, oxygenates, and α-olefins. Consequently, these

products serve as vital precursors to bulk commodities such as synthetic fibers, rubbers, plastics, lubricants, surfactants, and detergents.

Consequently, modifications to Fischer-Tropsch catalysts have been proposed. Modified Fischer-Tropsch synthesis represents an optimized advancement over conventional FTS. Its core strategy addresses the bottlenecks of traditional FTS, such as poor product selectivity, limited feedstock scope, and insufficient catalyst stability, through catalyst modification, feedstock adjustment, or process parameter optimization. This approach enables more efficient, targeted conversion of syngas (or CO_2 combined with green hydrogen).

The regulatory mechanism governing the strong interaction between metals/metal oxides and zeolites, which affects catalyst structure, reducibility, mass transfer performance, and catalytic activity, is the primary reason for the enhanced catalyst performance[53]. Furthermore, as illustrated in Figure 2D[54], the gas recycle ratio, a key process parameter, also plays a crucial role in regulating the reaction behavior of CO and H_2 conversion to C_5-C_{18} olefins during Fischer-Tropsch synthesis[55].

Cu-Co catalytic systems

Conventional Cu-based catalysts suffer from several inherent drawbacks, including low single-pass CO_2 conversion and severe side reactions via the RWGS pathway at elevated temperatures, which lead to insufficient methanol selectivity. Furthermore, these catalysts are prone to Cu species sintering, resulting in poor stability and unsatisfactory economic performance[56,57]. Introducing Co facilitates the formation of Co-Cu alloys and reduces Cu particle size, thereby suppressing carbon deposition, metal oxidation, and post-reaction structural evolution of the catalyst[58]. For simple CuCo catalysts without additives, surface hydroxyl groups on the support play a critical and irreplaceable role in the direct synthesis of ethanol from syngas[59]. The primary challenges for CuCo-based catalysts are constructing novel active sites for alcohol formation, suppressing hydrocarbon selectivity, and improving ethanol selectivity[36]. Figure 3A illustrates a plausible reaction pathway for n-butanol formation[60]. Taking Cu_6Co_3 as a typical example, Cu serves as a core regulatory component in the system compared with pure Co catalysts. Cu precisely modulates the size of Co active sites, inhibits C-O bond cleavage and the formation of hydrocarbon byproducts, stabilizes and enriches undissociated CO and HCO intermediates, and effectively lowers the energy barrier for the HCO insertion reaction[61]. Figure 3B shows the reaction network for higher-alcohol synthesis from syngas over the optimal bulk Co-Cu catalyst with a Co/Cu molar ratio of 2:1[62]. Dissociative CO adsorption produces chain-growth intermediates that either undergo β-H elimination to form olefins, which are then hydrogenated to alkanes, or undergo CO insertion to form oxygenated intermediates, which are subsequently hydrogenated to linear primary alcohols. Both hydrocarbon and alcohol products follow the same Anderson-Schulz-Flory chain-growth probabilities. Hydroformylation of ethylene to 1-propanol is a minor pathway that becomes significant only when the ethylene volume fraction exceeds 1 vol%, and its contribution to alcohol formation is negligible under conventional steady-state conditions. This reaction model enables a unified elucidation of the kinetic properties and surface adsorption behavior of bimetallic Co-Cu catalytic systems.

The catalytic conversion of syngas to ethanol and higher alcohols has emerged as a prominent research hotspot in C_1 chemistry. However, traditional CuCo-based catalysts often suffer from a broad product distribution and low ethanol selectivity. To address these limitations, Sun *et al.*[63] introduced Mn to modulate the catalyst architecture. The incorporation of Mn effectively inhibits Cu crystallite growth and enhances the dispersion of both Cu and Co species. Consequently, the resulting CuCoMn catalyst achieves highly selective direct synthesis of ethanol from syngas, attributed to its unique spherical lamellar morphology, Cu-Co synergy, and the promoting effect of Mn. Separately, Xiang *et al.*[64] systematically

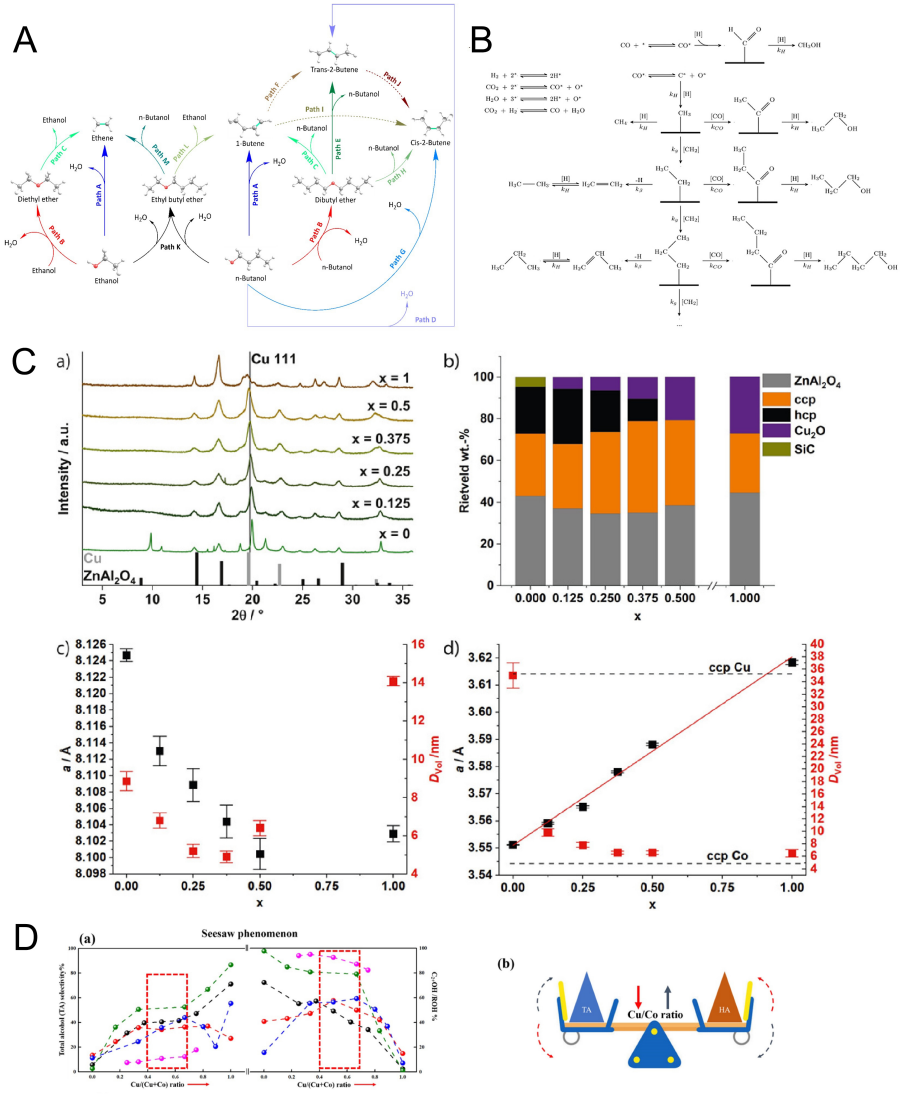

Figure 3. (A) Reaction scheme for n-butanol/ethanol dehydration and butene isomerization pathways in H-ZSM-5. (A) is reprinted with permission from Ref.[60], Copyright © 2024 Royal Society of Chemistry; (B) Simplified reaction scheme for the HAS over the CoCu catalyst. (B) is reprinted with permission from Ref.[62], Copyright © 2022 American Chemical Society; (C) Powder XRD analysis of the spent catalysts after CO hydrogenation at 20 bar-60 bar and 200-380 °C after passivation at room temperature with air. The complete pattern is visualized in (a), with the dark grey bars corresponding to the Cu (ccp) reference and the black bars corresponding to the $ZnAl_2O_4$ reference. The resulting quantification of the assigned phases by a Rietveld refinement is shown in (b). (c) Compositional dependence of the cell parameter and domain size of the spinel phase. (d) The ccp phase shows a significant expansion of the cell parameter with the copper content x. The red line is a linear fit to all data points; the dashed lines indicate the lattice parameters for bulk ccp Cu and Co taken from several entries of the ICSD (#627115, 627114, 622435, 44989). The apparent domain size shows a drastic initial decrease upon addition of copper in the catalyst system. (C) is reprinted with permission from Ref.[65], Copyright © 2022 Wiley-VCH GmbH; (D) Catalytic performance of CuCo catalysts varying Cu/Co ratio. (a) Catalytic performance of CuCo catalysts varying Cu/Co ratio; (b) Schematic diagram of "Seesaw" phenomenon [Note: the red and black arrows in (b)] represent the decrease and increase in Cu/Co ratio, respectively. (D) is reprinted with permission from Ref.[68], Copyright © 2024 MDPI. XRD: X-ray diffraction analysis.

investigated the regulatory effects of activation parameters on the catalytic performance of bimetallic CoCu catalysts under four distinct gaseous atmospheres. The results show that increasing cobalt loading simultaneously enhances intrinsic catalytic activity and the Anderson-Schulz-Flory (ASF) chain-growth probability. Modulating the Co/Cu molar ratio drastically alters the fundamental physicochemical properties of the catalysts. Based on the experimental data summarized in Table 1, the total number of surface Co active sites jointly determines the upper limit of chain-growth factors for oxygenates α(ROH) and hydrocarbons α(HC), while the Cu component merely tunes product branching selectivity. This observation directly

Table 1. Performance of different Co/Cu ratios

Catalyst	CO conversion (%)	Selectivity (wt%)				Probability of ASF chain growth		Reference
		ROH	RH	R=	CO_2	α(ROH)	α(HC)	
Co_1Cu_2	2.0	36.7	49.3	11.3	2.7	0.28	0.46	[64]
Co_1Cu_1	3.2	37.4	49.4	11.3	1.9	0.30	0.47	
Co_2Cu_1	5.7	37.9	50.5	10.2	1.4	0.33	0.47	
Co_4Cu_1	11.0	30.8	53.2	15.0	1.0	0.37	0.53	

ASF: Anderson-Schulz-Flory; ROH: alcohols; RH: alkanes.

verifies that the carbon chain-growth reaction exclusively proceeds on Co active sites. Consistent with trends from two sets of comparative experiments, increasing the Co fraction improves CO conversion and hydrocarbon selectivity but markedly suppresses alcohol formation. Conversely, a higher Cu/Co ratio not only boosts catalytic activity but also facilitates selective alcohol synthesis, increasing the methanol proportion in liquid-phase products. Figure 3C presents the Rietveld-refined X-ray Diffraction (XRD) patterns of passivated spent Cu-Co/$ZnAl_2O_4$ catalysts, which visually demonstrate the regulatory effect of Cu doping ratio on phase composition, crystal structure, and metal micromorphology[65]. The $ZnAl_2O_4$ spinel support remains stable throughout all samples with a mass fraction of approximately 40%. The lattice parameter of spinel shrinks with increasing Cu content, originating from the substitution of lattice Zn^{2+} by Co^{2+} and thereby the SMSI. The monometallic Co catalyst contains both hcp and ccp metallic phases, with a metal domain size of 35 nm[66]. Incorporation of a small amount of Cu drastically refines metal crystallites, and only the ccp metallic phase is retained in Cu-containing samples, with domain size gradually decreasing to 6.5 nm as Cu proportion rises. The linear expansion of ccp lattice parameters with Cu content confirms that the hydrotalcite precursor generates intimate nanoscale Cu-Co contact interfaces that form alloy-like active sites, balancing CO dissociative and associative adsorption[62]. Only minor Cu_2O originating from air passivation is detected in Cu-doped samples, without crystalline cobalt carbides. The introduction of Cu reconstructs metal crystal forms, suppresses sintering of active metal particles, and significantly alleviates carbon deposition over Co sites via bimetallic interfacial effects, further optimizing the catalytic stability for higher alcohol synthesis from the microstructural perspective.

To address the challenges of mismatched electronic structures, facile agglomeration of active sites, and low ethanol selectivity in CuCo catalysts, Sun *et al.*[67] systematically elucidated, for the first time, how N-doping levels and calcination temperatures regulate the electronic synergy of CuCo and ethanol selectivity. In summary, the incorporation of various metals can significantly enhance the catalytic performance and target-product selectivity of CuCo-based catalysts. However, higher loadings of the introduced metal do not always yield better results; rather, an optimal concentration exists. Furthermore, metal doping can effectively boost overall catalytic activity, while the Co/Cu ratio and activation conditions also play a crucial role in determining catalytic performance [Figure 3D][68].

Catalytic screening was carried out under 240 °C, 40 bar and an H_2/CO feed ratio of 1.5. CoCu catalysts were synthesized by thermally decomposing oxalate precursors in a continuous H_2 stream at 370 °C.

Cu-Fe catalytic systems

Establishing dense and robust interfacial interactions between metallic components is essential for designing efficient catalytic systems. However, Fe-Cu bimetallic catalysts often suffer from intrinsically poor interfacial contact efficiency. Consequently, particle agglomeration and phase separation readily occur during operation, leading to rapid passivation or structural degradation of surface-active sites and resulting in interfacial instability[69]. These challenges ultimately trigger a continuous decline in catalytic activity, or even

complete deactivation, thereby severely restricting the long-term stability and industrial viability of Fe-Cu-based catalysts. Furthermore, monometallic counterparts have inherent limitations: Fe-based catalysts typically show inadequate low-temperature activity, whereas Cu-based catalysts are highly prone to thermal sintering at elevated temperatures.

Conversely, the synergistic interaction between Fe and Cu in bimetallic systems effectively addresses these limitations. Specifically, Cu significantly lowers the reduction temperature of Fe, thereby facilitating mild activation, while Fe promotes the dispersion of Cu species to prevent sintering and enhance structural stability. This synergy allows the catalyst to preserve surface oxygen vacancies and active interfacial structures under *in situ* mild reduction conditions, ultimately delivering superior low-temperature catalytic activity[70,71].

Chen *et al.*[69] synthesized a series of Mg-modified FeCu-based catalysts with varying Mg contents via a co-precipitation method. They found that introducing an appropriate amount of Mg effectively suppressed metal particle agglomeration and improved dispersion. This modification regulated the catalyst's structure, interfacial activity, and adsorption properties, thereby enhancing catalytic selectivity and product yield. In a related study, Ding *et al.*[72] prepared CuFeMnZnO catalysts by co-precipitation, followed by impregnation with a potassium (K) promoter (using KNO_3 at loadings of 0, 0.2, 0.5, 1.0, and 1.5 wt.%). Their results showed that the K promoter facilitated the migration of bulk iron species to the catalyst surface and strengthened Fe-Cu interactions. However, it also reduced specific surface area and hindered the reduction of Cu and Fe. Optimal catalytic performance was achieved at a K loading of 0.5 wt.%; however, excessive loading (> 0.5 wt.%) reduced activity due to active-site blockage. Furthermore, Jiang *et al.*[73] systematically investigated CO_2 conversion via Fischer-Tropsch synthesis using carbon-supported iron-based catalysts, employing three modification strategies: screening iron salt precursors, doping with a K promoter, and co-adding organic ligands. These modifications optimized the dispersion of active components, regulated the active-phase composition, and improved surface adsorption properties, enabling efficient CO_2 conversion with C_{5+} hydrocarbon selectivity up to 55%. A subsequent study by Xu *et al.*[74] further confirmed that these modification strategies and their underlying mechanisms are equally applicable to the hydrogenation of CO_2 to higher alcohols. Modulating structure, interface, and adsorption with Mg, Mn, and K alleviates deactivation in FeCu-based catalysts. Mg isolates metal particles to suppress sintering and carbon deposition[75]; Mn stabilizes the lattice and anchors active components[76]. Appropriate K enriches surface Fe species and strengthens Fe-Cu interaction, while excess K covers active sites and hinders metal reduction. For carbon-supported Fe catalysts, K synergizes with iron precursors and organic ligands to tune active phases and reduce carbon deposition. This modification strategy is feasible for CO_2 hydrogenation to long-chain hydrocarbons and higher alcohols.

In summary, optimizing preparation methods and incorporating metal promoters can effectively enhance catalytic performance. However, metal promoters have an optimal doping concentration; excessive addition tends to block active sites, thereby compromising catalytic activity. For example, varying the Fe/Cu ratio significantly affects catalytic efficiency. Experimental evidence indicates that optimal performance is achieved at a Fe/Cu molar ratio of 1:1, with deviations from this ratio resulting in diminished catalytic effectiveness[77].

Modified methanol synthesis catalyst

Smith and Anderson first described the chain-growth process for alcohol synthesis from syngas over modified methanol catalysts in 1982 as a 1-2 carbon-addition mechanism involving α- and β-carbons[78]. As shown in Figure 4A, the synthesis of liquid fuels from CO_2 and H_2 follows various catalytic pathways that cover core reactions, key catalysts, intermediates, and applications. This forms a classic technical roadmap

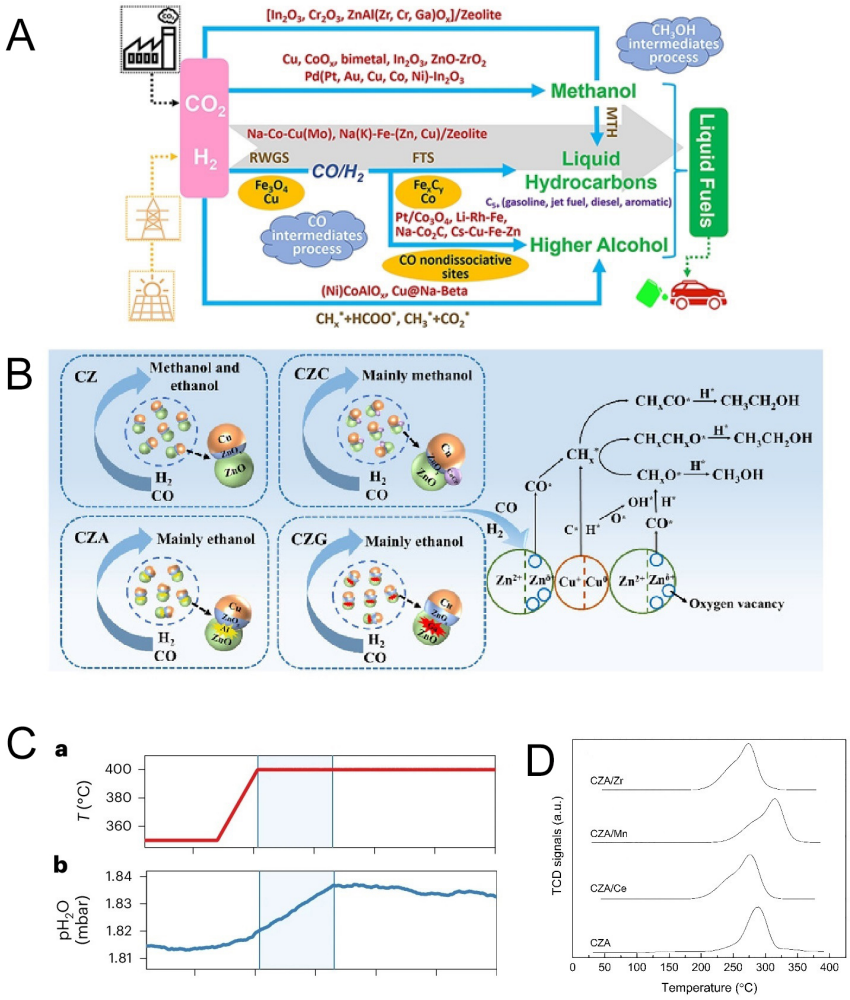

Figure 4. (A) Novel Heterogeneous Catalysts for CO_2 Hydrogenation to Liquid Fuels. (A) is reprinted with permission from Ref.[79], Copyright © 2020 American Chemical Society; (B) CO hydrogenation mechanism over catalysts to $C_{2+}OH$. (B) is reprinted with permission from Ref.[80], Copyright © 2026 WILEY; (C) Evolution of the Cu lattice parameter at 400 °C in H_2:CO_2 = 1:1 feed. (a) Temperature profile. (b) H_2O partial pressure. The conditions are as follows: gas composition H_2:CO_2:He = 2:2:1, pressure 661 mbar, heating rate 10 K min^{-1}, electron dose rate 3.4 $e^- Å^{-2} s^{-1}$. (C) is reprinted with permission from Ref.[82], Copyright © 2026 Springer Nature; (D) H_2-TPR profiles of the calcined catalysts. (D) is reprinted with permission from Ref.[88], Copyright © 2024 WILEY. CZ: CuZn; CZA: CuZnAl; CZC: CuZnCr; CZG: CuZnGa; TPR: temperature-programmed reduction.

for CO_2 resource utilization[79]. Figure 4B systematically illustrates the reaction pathways of CO hydrogenation to C_{2+} alcohols over the catalysts[80]. Differences in product distribution for syngas hydrogenation to alcohols over four CuZn-based catalysts (CZ: CuZn, CZA, CZC:CuZnCr, and CZG: CuZnGa) clarify the synergistic catalytic mechanism involving multiple active sites. From the perspective of the microscopic reaction process, Cu^0 mediates CO dissociation to generate CH_x species; oxygen vacancies cooperate with Cu^+ to capture CO and form CH_xO intermediates via non-dissociative adsorption. $Zn^{\delta+}$ serves as the functional site for C-C coupling, driving the combination of CHx and CHxO to produce C_2 intermediates, which are further hydrogenated into ethanol. When $Zn^{\delta+}$ coupling sites are scarce, CH_xO^* tends to be directly hydrogenated to methanol. These findings establish a progressive structure-activity relationship: promoters modulate the concentration of oxygen vacancies; oxygen vacancies coordinate the synergistic behavior of multiple active sites; and the spatial distribution of active sites regulates the carbon-chain-length distribution of alcohol products.

Historically, modified methanol synthesis catalysts can be classified into two main categories. High-temperature catalysts are primarily composed of $ZnCrO_x$ and $MnCrO_x$ systems doped with alkali metal promoters, which deliver a higher ratio of higher alcohols to methanol and eliminate the need for methanol recycling. Conversely, low-temperature catalysts represented by Cu/ZnO and Cu/Zn/Cr systems have emerged as the industrial mainstream for CO_2 hydrogenation to methanol, benefiting from mild reaction conditions and the cost-effectiveness of copper-based components. Among them, $Cu/ZnO/Al_2O_3$ is the most widely adopted low-temperature copper-based catalyst, and the dynamically reversible synergistic interaction between Cu and Zn species is the primary origin of its superior methanol catalytic activity, distinguishing it from high-temperature Cr-based catalysts[81]. As illustrated in Figure 4C, the *in situ* generated H_2O during catalysis drives the re-oxidation of transient CuZn alloys, which restores the Cu lattice parameter to the benchmark value of pure Cu and enables the continuous reversible interconversion between CuZn alloys and Cu-ZnO interfacial sites, thereby stabilizing the dynamic equilibrium required for catalytic cycles[82]. This unique dynamic redox cycle mechanism microscopically explains why low-temperature copper-based CZA catalysts are more suitable for directional methanol synthesis than high-temperature Cr-based counterparts, which in turn sustains stable catalytic activity toward CO_2 hydrogenation over long-term operation and is fully consistent with their outstanding methanol synthesis performance under steady-state conditions.

Historically, modified methanol synthesis catalysts were divided into two categories. High-temperature catalysts, primarily $ZnCrO_x$ and $MnCrO_x$+K/Cs, are noted for their high higher-alcohol-to-methanol ratio and the absence of a methanol recycling requirement. Conversely, low-temperature catalysts, such as Cu/ZnO and Cu/Zn/Cr+Cs/K, benefit from milder reaction conditions and the cost-effectiveness of Cu-based components.

He *et al.*[83] prepared a quaternary $Cu/ZnO/ZrO_2/MgO$ catalyst via a co-precipitation method. The introduction of Mg significantly optimized the catalyst's microstructure, improved the dispersion of active components, and created appropriate basic sites. In terms of microstructure, Mg inhibited the agglomeration of CuO and ZnO particles, reducing particle size, increasing specific surface area and pore volume, and enhancing active-site exposure[84]. Furthermore, it regulated surface properties by constructing medium-strong basic sites, which strengthened CO_2 adsorption and activation. Additionally, Mg promoted inter-species interactions, specifically enhancing the synergy between Cu and ZnO, which improved the dispersion and reducibility of Cu species, increased the content of chemisorbed oxygen, and ultimately optimized catalytic activity.

Traditional $Cu/ZnO/Al_2O_3$ catalysts still have room for performance improvement, as water produced during the reaction can induce the sintering and deactivation of Cu and ZnO. Therefore, it is imperative to develop Cu-based catalysts with both high activity and high stability. The catalytic activity of bifunctional hybrid catalysts is closely linked to the reducibility of copper oxide in the calcined products. Introducing ZrO_2 into the Cu-ZnO catalyst system can effectively enhance the reducibility of copper oxide and significantly lower its reduction temperature[85]. Chang *et al.*[86] fixed the mass fraction of Cu at 30% to investigate the regulatory effect of the ZnO/ZrO_2 mass ratio on catalytic performance. The results revealed that the ratio drastically modulates the catalyst microstructure (CuZn alloy formation and Cu dispersion) and surface adsorption properties (the number of active CO_2 adsorption sites). According to the data summarized in Table 2, the CO_2 desorption capacity, surface metallic Zn^0 (CuZn alloy) content, and methanol space-time yield all exhibited typical volcanic trends, with the optimal catalytic performance achieved over the C3Z2Z5 catalyst at a $ZnO:ZrO_2$ mass ratio of 2:5. In Zn-poor and Zr-rich systems, increasing the ZnO proportion facilitates CuZn alloy generation, enriches Cu-ZrO_2 interfaces and CO_2 activation sites, and thus continuously elevates catalytic activity. Once the ratio exceeds 2:5, insufficient ZrO_2 content drastically reduces Cu-ZrO_2 interfaces and aggravates Cu particle agglomeration, simultaneously lowering CO_2 adsorption capacity and CuZn alloy

content, which deteriorates catalytic activity. These volcanic profiles arise from the synergistic balance between two types of active sites: CuZn alloys and Cu-ZrO_2 interfaces. The maximum catalytic performance is achieved when the synergistic effect of these two sites reaches an optimal balance. The synergistic effect between Cu and oxides (ZnO, ZrO_2), particularly through the CuZn alloy and Cu-ZrO_2 interface, is crucial for enhancing the catalytic performance of CO_2 hydrogenation to methanol and provides a theoretical basis for designing high-efficiency catalysts[87].

Zr does not incorporate into the precursor lattice; instead, it integrates into the ZrO_2 lattice to form a solid solution after calcination. As shown in Figure 4D, modification with CeO_2 and ZrO_2 lowers the reduction temperature of CuO and improves catalyst reducibility[88]. Among all samples, CZA/Zr exhibits the lowest reduction peak temperature. The strong interaction between MnO_2 and Cu species significantly shifts the reduction peak toward higher temperatures, inhibiting CuO reduction. The reducibility follows the order: CZA/Zr > CZA/Ce > CZA > CZA/Mn, which directly corresponds to the differences in Cu dispersion over various catalysts and elucidates the intrinsic origin of their distinct low-temperature catalytic activities. Furthermore, López-Luque *et al.*[89] found that the methanol formation rate shows a volcanic trend with the surface spacing of Cu nanoparticles. Thus, in addition to mass ratio and doping elements, particle spacing is another critical design parameter for metal-oxide interface catalysts.

Mo-based catalyst

Mo-based catalysts exhibit remarkable sulfur tolerance during the conversion of CO to higher alcohols. They can tolerate trace sulfur impurities in feedstocks, thereby avoiding the need for stringent desulfurization pretreatment and broadening their practical applicability. Furthermore, their selectivity can be precisely tailored through modification strategies, including alkali metal doping, transition metal incorporation, and support optimization[90]. However, these reactions typically require harsh operating conditions (high temperature and pressure), and selectivity toward target products remains suboptimal, limiting their industrial viability[91].

In the direct synthesis of higher alcohols from syngas, Mo-based catalysts face the dual challenges of harsh reaction conditions and suboptimal product selectivity. Conventional Mo-based catalytic systems typically operate at temperatures exceeding 300 °C and pressures above 80 bar, where methanol is the dominant product, severely limiting the effective generation of C_{2+} alcohols[92]. Consequently, developing Mo-based catalysts that achieve high C_{2+} alcohol selectivity under milder conditions, especially at low pressure, holds substantial scientific significance and practical value.

In industrial practice, implementing low-pressure reaction conditions not only significantly reduces energy consumption but also simplifies facility design and decreases operational and maintenance costs. This approach simultaneously enhances both the environmental sustainability and economic competitiveness of the process, providing critical technical support for the green, large-scale production of higher alcohols[93]. Mo-based catalysts hold significant promise for converting syngas to higher alcohols because of their abundant availability and remarkable sulfur tolerance. However, their product selectivity and space-time yield still necessitate further improvement[94]. Molybdenum sulfide-based catalysts have long been a primary research focus for mixed alcohol synthesis owing to their outstanding sulfur tolerance and high activity in the water-gas shift reaction, making them appealing candidate catalysts for this reaction[95,96]. Because mixed alcohol synthesis is often coupled with the reverse water-gas shift process, efficient CO_2 conversion helps tune product distribution. Related investigations on molybdenum-based catalysts further reveal that unsaturated molybdenum oxide ($Mo_{17}O_{47}$) delivers high activity toward the reverse water-gas shift reaction without pre-carburization, while maintaining stable operation at 600 °C over 2,000 h[97]. Accordingly, this review focuses on two prominent catalyst classes: Mo-S and Mo-C systems.

Table 2. Performance comparison of Cu/ZnO/ZrO_2 catalysts with different ZnO/ZrO_2 mass ratios

Catalysts	The mass ratio of ZnO to ZrO_2	Content of Cu (wt%)	Specific surface area (m^2/g)	Aperture (nm)	Cu dispersion (%)	Cu Particle size (nm)	H_2 adsorption capacity ($mmol/g_{cat}$)	CO_2 desorption amount ($mmol/g_{cat}$)	Key features	Reference
C3Z0Z7	0:7	28.62	95.5	13.0	14.6	13.10	0.0147	0.244	No ZnO, only Cu-ZrO_2 interface, moderate CO_2 desorption amount	[86]
C3Z1Z6	1:6	28.89	94.4	13.1	21.9	8.82	0.0147	0.278	The CuZn alloy content is relatively low, while CO_2 desorption is relatively high	
C3Z2Z5	2:5	30.80	88.7	15.2	25.2	8.18	0.0148	0.311	The CuZn alloy has the best interface synergy with Cu-ZrO_2, and the CO_2 desorption amount is the highest	
C3Z3Z4	3:4	30.73	80.5	17.1	28.9	7.13	0.0139	0.250	The CuZn alloy has an appropriate content, and its catalytic performance is second only to C3Z2Z5	
C3Z4Z3	4:3	28.54	71.5	21.9	38.0	5.02	0.0141	0.203	The content of ZrO_2 decreases, and the Cu-ZrO_2 interface decreases	
C3Z5Z2	5:2	28.19	71.0	20.0	33.3	5.67	0.0155	0.180	The content of ZnO is relatively high, and the tendency of Cu particles to aggregate is obvious	
C3Z6Z1	6:1	30.22	70.7	21.0	38.3	5.29	0.0161	0.117	The content of ZrO_2 is extremely low, and the amount of CO_2 desorption has significantly decreased	
C3Z7Z0	7:0	31.13	30.7	28.6	-	0.97	0.0092	0.061	Without ZrO_2, only the Cu-ZnO system was used. Cu dispersion was poor, and adsorption capacity was the lowest	

Mo-S catalyst

Molybdenum disulfide (MoS_2)-based sulfides are a class of non-noble metal catalytic materials with significant industrial potential. Their most prominent advantage is excellent sulfur tolerance, which enables direct use with crude sulfur-containing syngas feedstocks without pre-desulfurization, thereby simplifying the overall process flow and reducing production costs. Numerous studies have shown that alkali metals (e.g., potassium) can act as modification promoters that simultaneously optimize intrinsic catalytic activity and the directional synthesis of higher alcohols in MoS_2[98]. Catalytic performance depends strongly on atomic-scale regulation of MoS_2's layered nanostructure. Specifically, the type and abundance of interlayer and edge sulfur vacancies, as well as the stacking number of two-dimensional nanosheets, are key regulatory targets for product distribution in syngas conversion[99,100]. From the perspective of microscopic reaction mechanisms, Mo edge sulfur vacancies tend to drive CO insertion and promote C-C coupling reactions, facilitating preferential ethanol formation. Conversely, basal plane sulfur vacancies dominate the single-carbon hydrogenation pathway and are conducive to methanol generation[101]. Nevertheless, excessive disordered sulfur vacancies can induce complete cleavage of C-O

bonds, markedly increasing selectivity toward low-carbon hydrocarbons such as methane. Accordingly, directional modulation of the main product distribution in syngas conversion can be achieved by precisely regulating the interlayer sulfur vacancy density and nanosheet morphology of MoS_2[102,103].

MoS_2-based sulfide catalysts inherently possess outstanding resistance to sulfur poisoning and carbon deposition. Precise construction of interlayer sulfur vacancies via metal doping and layered-structure regulation enables directional optimization of carbon-chain growth efficiency and higher alcohol selectivity. Cobalt promoters can reconstruct edge sulfur vacancies in MoS_2 nanosheets, forming highly active Co-Mo-S sites that substantially improve the selectivity of C_{2+} alcohols and the space-time yield of total alcohols. However, the formation of inert Co_9S_8 phases disrupts the ordered sulfur-vacancy structure and deteriorates catalytic activity[104]. Li *et al.*[105] verified that pure hydrogen pretreatment can generate sulfhydryl groups at the edges of Co-Mo-S nanosheets. Electron transfer at sulfur sites anchors Co atoms, inhibits the precipitation of inert Co_9S_8, and stabilizes the configuration of interlayer sulfur vacancies, providing a theoretical basis for the activation mechanism of MoS_2-based catalysts. For potassium-doped modified systems, intercalation of K species into MoS_2 nanosheets expands the interlayer spacing, remodels interlayer sulfur vacancies and coordinatively unsaturated sites, and forms tightly coupled MoS_2/$KMoS_2$ heterogeneous dual-active interfaces. Figure 5A compares the evolution of surface species, intermediate distribution, and reaction pathways over ER-MoS_2-K and PD-MoS_2-K during hydrogen pretreatment and CO hydrogenation[106]. Edge-rich ER-MoS_2-K generates abundant edge sulfur vacancies upon H_2 reduction, which efficiently facilitate C-O cleavage of CH_xO intermediates to produce CH_x species. The C-C coupling intermediate CH_xCO is captured, directing the reaction pathway toward carbon chain growth for the synthesis of higher alcohols such as ethanol. This catalyst exhibits lower activation energy for methanol hydrogenation and superior C-O dissociation activity. Conversely, plane-dominated PD-MoS_2-K mainly possesses in-plane sulfur vacancies[107]. CH_3O species readily undergo hydrogenation and desorption to form methanol, so they fail to accumulate stable C-C coupling intermediates; thus, the reaction pathway is dominated by methanol formation. Accordingly, the population and spatial distribution of sulfur vacancies dictate catalyst selectivity for lower and higher alcohols.

Furthermore, the support plays a pivotal role in catalyst architecture. The alcohol product distribution over MMO-supported catalysts deviates significantly from the ASF distribution, exhibiting a distinct profile compared with the typical distribution of ethanol, n-propanol, and n-butanol. Notably, this catalyst yields the highest chain growth factor (α) among all samples, indicating a markedly enhanced probability of long-chain alcohol formation, substantial suppression of methanol production, and a pronounced preference for C_{3+} alcohols[108].

Mo-C catalyst

In recent years, research on Mo-based catalysts has increasingly focused on the Mo_2C system. Compared with MoC-based catalysts, Mo_2C-based catalysts exhibit superior total alcohol selectivity, largely due to abundant non-dissociative CO adsorption sites. Nevertheless, low CO conversion and insufficient selectivity toward higher alcohols remain significant bottlenecks that hinder the large-scale industrial application of Mo_2C-based catalysts[109,110]. Figure 5B presents schematic diagrams of three typical structures on the Mo_2C surface, namely Mo^0 sites formed via over-reduction, carbon vacancy defects, and molybdenum vacancy defects, which visually distinguish the Mo species and coordination environments associated with different defects[111]. Coordinatively unsaturated Mo sites adjacent to carbon vacancies serve as the core active sites for CO hydrogenation to mixed alcohols. Conversely, Mo^0 species are readily oxidized to catalytically inactive high-valent Mo^{6+} during catalyst passivation, leading to inferior catalytic activity[112]. Mo species associated with molybdenum vacancy defects also show weak catalytic performance. Both Mo^0 and Mo vacancy defects

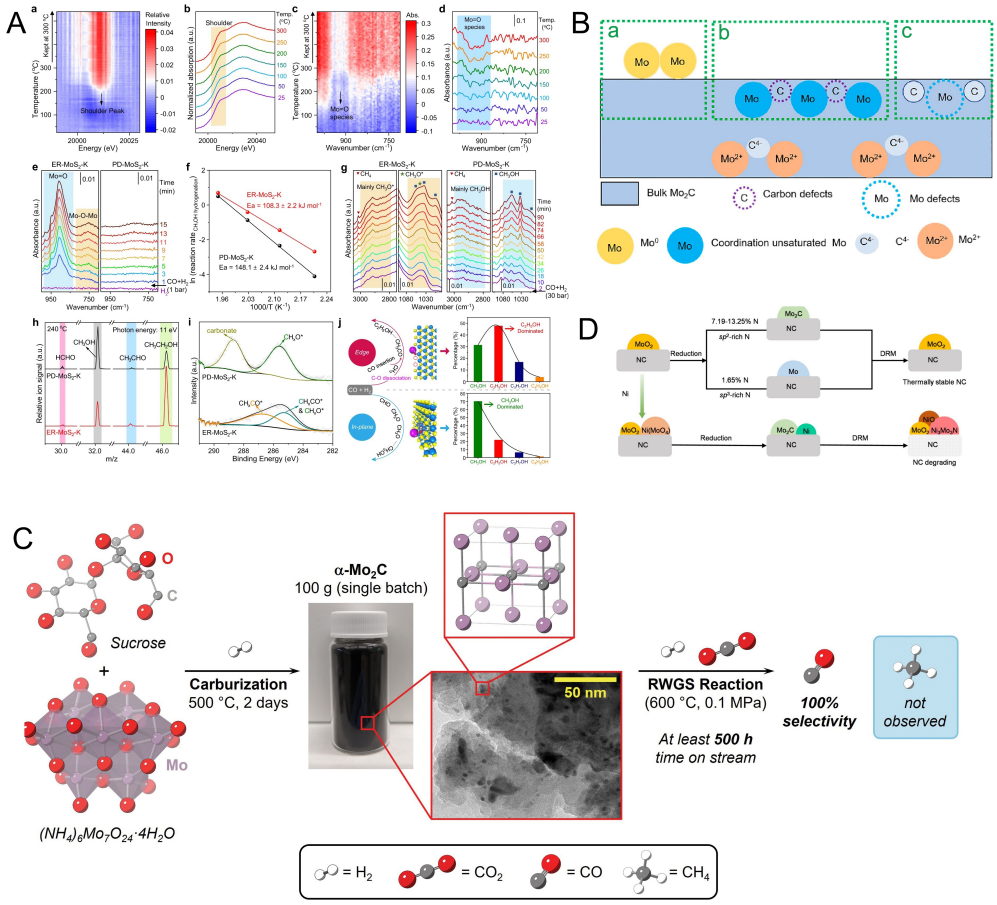

Figure 5. (A) *In situ* ED-XAS: (a and b) coupling *in situ* DRIFTS; (c and d) characterizations of ER-MoS_2-K during H_2 pretreatment measured with a hyphenated technology. Relative intensity in (a) was obtained by subtracting each spectrum from the first spectrum. (e) *In situ* DRIFT spectra of CO hydrogenation over the H_2-pretreated catalysts at 25 °C, H_2/CO of 2 and 1 bar. (f) Arrhenius plots calculated based on the reaction rate for methanol hydrogenation over PD-MoS_2-K and ER-MoS_2-K. (g) *In situ* DRIFT spectra of CO hydrogenation over the H_2-pretreated catalysts at 240 °C, H_2/CO of 2 and 30 bar. (h) *In situ* SVUV-PIMS detection of the CO hydrogenation intermediates and products over the H_2-pretreated catalysts at 240 °C, H_2/CO of 2 and 5 bar. (i) Quasi *in situ* SRPES detection of the CO hydrogenation intermediates. SRPES spectra were obtained after the treatment of the H_2-treated catalysts with reaction gas (H_2/CO = 2) at 240 °C and 5 bar for 0.5 h. (j) Proposed reaction mechanism for CO hydrogenation to methanol and ethanol on edge and in-plane sites of MoS_2. (A) is reprinted with permission from Ref.[106], Copyright © 2023 Springer Nature; (B) Schematic diagram of Mo_2C surface. (a) Mo^0, (b) carbon defects and (c) Mo defects. (B) is reprinted with permission from Ref.[111], Copyright © 2021 MDPI; (C) Schematic of catalyst synthesis process and its performance for RWGS reaction. (C) is reprinted with permission from Ref.[113], Copyright © 2024 The American Association for the Advancement of Science; (D) Transformations of Mo/NC and Ni-Mo/NC catalysts after H_2 reduction and DRM reaction. (D) is reprinted with permission from Ref.[114], Copyright © 2025 WILEY. RWGS: Reverse water-gas shift; ED-XAS: Energy-dispersive x-ray absorption spectroscopy; DRIFTS: diffuse reflectance infrared fourier-transform spectroscop; DRM: dry reforming of methane; NC: nitrogen-doped carbon; SRPES: synchrotron-radiation photoelectron spectroscopy.

tend to promote complete CO dissociation, producing substantial hydrocarbon by-products. This schematic clearly establishes the correlation among carbon vacancy defects, coordinatively unsaturated Mo sites, and activity toward alcohol synthesis. Furthermore, it elucidates the intrinsic mechanism underlying the volcano-type variation in catalytic performance upon Ni doping-induced modulation of lattice carbon content from the perspective of defects. This study provides visualized theoretical support for understanding the structure-activity relationship among lattice carbon content, surface defects, and catalytic selectivity.

Figure 5C illustrates the facile, scalable synthesis of cubic α-Mo_2C catalysts, along with a schematic of their application in the high-temperature RWGS reaction[113]. Nanocrystalline α-Mo_2C was directly synthesized by carburization under an H_2 atmosphere at 500 °C, utilizing ammonium molybdate as the molybdenum precursor and sucrose as a sustainable carbon source. Under RWGS reaction conditions (600 °C, 0.1 MPa),

Table 3. Comparison of catalytic performances of different catalysts

Catalyst	CO conversion rate (%)	Selective alcohol property (%)	The proportion of C_{2+} alcohols among alcohols (%)	Methane selectivity (%)	Reaction pressure (MPa)	Reference
Mo_2C	51.3	1.1	17.3	-	3	
Rh/Mo_2C	65.2	4.2	1.5	56.9	3	
K/Mo_2C	14.0	30.8	-	-	3	[115]
RhK/Mo_2C	9.9	44.4	85.6	20.7	1	
RhK/Mo_2C	20.2	51.4	71.0	20.7	3	

this catalyst achieved 100% CO selectivity and maintained exceptional stability for over 500 h. Conversely, β-Mo_2C can undergo electron transfer with Pd, forming SMSI.

Promoter doping remains a mainstream strategy for modifying Mo_2C-based catalysts. Figure 5D illustrates the phase evolution, variations in active centers, and deactivation pathways of N-doped carbon-supported Mo_2C and Ni-Mo bimetallic catalysts during H_2 reduction and dry reforming of methane (DRM)[114]. This schematic clearly explains how N species and Ni promoters regulate the valence state and crystal phase of Mo species, as well as the mechanisms governing catalyst stabilization and deactivation. Although introducing Ni can facilitate reduction via hydrogen spillover and enhance initial catalytic activity, it also oxidizes Ni and Mo_2C, triggers formation of the inert Ni_3Mo_3N phase, and accelerates gasification and degradation of carbon supports, ultimately leading to rapid catalyst deactivation.

Wang *et al.*[115] proposed a strategy to enhance the CO insertion capability of Mo_2C-based catalysts by introducing $Rh^{\delta+}$ and K species, achieving excellent catalytic performance for higher alcohol synthesis (HAS) at a mild reaction pressure of 1.0 MPa. As shown in Table 3, RhK/Mo_2C demonstrates optimal overall performance under identical reaction conditions. It maintains high alcohol selectivity even at low pressure, with significantly lower methane by-product selectivity compared to Rh/Mo_2C. Consequently, co-modification with Rh and K significantly improves the HAS performance of Mo_2C catalysts, enabling them to achieve 44.4% alcohol selectivity at low pressure and overcoming the traditional reliance of Mo-based catalysts on high-pressure conditions.

Conversely, Yang *et al.*[109] employed K and Ni as promoters. As in previous studies, the synergistic effect between K and Ni significantly enhanced the catalytic performance of Mo_2C. Among the tested catalysts, $KNiMo_2C/Al_2O_3$ exhibited the optimal performance, achieving a total alcohol selectivity of 67.6% and a remarkably high C_{2+} alcohol selectivity of 56%. Meng *et al.*[94] also synthesized a series of K- and Ni-promoted Mo_2C-based catalysts via impregnation; however, they used lignin-derived carbon as the support. As highlighted in Table 4, dual promotion with K and Ni is crucial for enhancing higher-alcohol selectivity in Mo_2C-based catalysts. Furthermore, catalytic performance is closely tied to support architecture: mesoporous structures facilitate mass transfer, whereas support-metal interactions influence active-site formation. Consequently, reaction conditions must be tailored to catalyst characteristics: milder temperatures and pressures favor alumina supports, whereas higher temperatures and pressures better suit the highly active sites of lignin carbon supports. Additionally, He *et al.*[110] successfully fabricated Mo_2C catalysts with a three-dimensional hierarchical porous (3DHP) structure using a hard-template method, which significantly optimized the specific surface area, pore architecture, and active site distribution. The synergistic effect between the 3DHP structure and K modification proved pivotal for performance enhancement, offering novel insights for designing high-efficiency Mo_2C-based HAS catalysts and broadening the application scope of 3DHP materials.

Table 4. Comparison of the performance of the two catalysts

Catalysts	Mo_2C/Al_2O_3	Mo_2C@LC
References	[109]	[94]
Carrier type	γ-Al_2O_3	LC
Carrier characteristics	Specific surface area: 121 m^2/g, mesoporous structure (pore diameter: 29 nm), pore volume: 1.23 cm^3/g	Specific surface area: 615.6 m^2/g, open mesoporous structure (pore diameter: 5.0 nm), pore volume: 0.22 cm^3/g, with defective carbon structure
Catalyst preparation	Excessive impregnation method + programmed temperature carbonization (at 700 °C in N_2 atmosphere), M/Mo atomic ratio 0.2, stepwise loading of Mo and K/Ni	Impregnation method + programmed temperature carbonization (at 850 °C in an atmosphere of 10% H_2/N_2), Mo/K = 5/1, Mo/Ni = 2/1. It can be impregnated separately or simultaneously
The role of key additives	K: Increases the crystallinity of β-Mo_2C, increases the proportion of high-valent Mo (Mo^{6+}), and enhances the non-desorbed adsorption of CO Ni: Reduces the reduction temperature of Mo oxides, promotes the formation of Mo^{2+}, and catalyzes the water-gas shift (WGS) reaction	K: Increases the proportion of high-valence Mo (Mo^{5+}/Mo^{6+}), enhances the catalyst's alkalinity, and promotes the growth of carbon chains Ni: Facilitates Mo reduction through hydrogen overflow, increases the size of Ni particles, and balances hydrogenation capacity with carbon chain growth
Reaction conditions	Temperature: 300 °C, Pressure: 3.0 MPa, H_2/CO = 2	Temperature: 340-380 °C, Pressure: 7.0 MPa, H_2/CO = 1
Optimal catalyst	$KNiMo_2C/Al_2O_3$	Ni/K/Mo_2C@LC
Catalytic performance	CO conversion rate: 7.2% Total alcohol selectivity: 67.6% C_{2+} alcohol selectivity: 56% (ethanol accounts for 37%) STY: 64.84mg/g_{cat}h (0.065g/g_{cat}h)	CO conversion rate: 47.9% (Ni/K/Mo_2C@LC_{500})/23.0% ($NiKMo_2C$@LC) Total alcohol selectivity: 57.9% C_{2+} alcohol selectivity: 76.7% (ethanol accounts for 50.9%) STY: 0.455 g/g_{cat}h (380 °C)
Stability	The continuous reaction lasted for 80 h, and the CO conversion rate and product selectivity remained stable	The reaction was carried out continuously for 100 h. The characteristic peaks of Mo_2C and Ni were retained, and the ethanol proportion remained at approximately 40%
Core advantage	The reaction conditions are mild (low temperature and low pressure), with high overall alcohol selectivity and a significant inhibitory effect of methanol	The space-time production rate is extremely high (7 times that of the left), and the carrier is resource-based (utilizing paper waste), with a high proportion of C_{2+} alcohols
Insufficiency	The STY value is low, the CO conversion rate is also low, and the carrier has no resource utilization value	The reaction pressure is quite high (7 MPa), and it requires a high temperature (380 °C) to achieve the optimal performance

STY: Space-time yield; LC: lignin carbon.

Mixed alcohols can serve not only as clean fuels that substitute fossil energy but also as solvents, chemical intermediates, and gasoline additives, and directly producing them from synthesis gas (syngas, H_2 + CO) - typically generated through the pyrolysis and gasification of carbonaceous feedstocks such as coal and biomass - realizes the clean and efficient utilization of carbon resources[111]. At the heart of this syngas-to-alcohol process lie the thermally driven decomposition that releases syngas and the subsequent dissociation and activation of reactant molecules on the catalyst surface; in particular, the C-O bond of CO must be activated in a controlled manner, so that the balance between dissociative CO adsorption and non-dissociative CO insertion directs the growing surface intermediates toward alcohols rather than hydrocarbons. Molybdenum carbide (Mo_2C) is well suited to this activation chemistry because of its noble-metal-like electronic structure, in which the insertion of carbon atoms into the Mo lattice elongates the Mo-Mo distance, contracts the Mo 4d orbitals, and enriches the density of states near the Fermi level[116]. Shou *et al.*[112] further showed that Ni doping promotes CO hydrogenation to mixed alcohols on Mo_2C: Ni inhibits the agglomeration of Mo_2C crystallites and suppresses surface carbon deposition, thereby enlarging the active surface area, whereas the electron transfer from Ni to Mo increases the electron cloud density of the Mo species and favors the non-dissociative adsorption and insertion of CO. More importantly, decreasing the number of carbon atoms in the Mo_2C lattice on the catalyst surface generates coordination-unsaturated molybdenum species that exhibit higher catalytic activity and mixed-alcohol selectivity; among the catalysts examined, MC-Ni-1.5 (Ni/Mo = 1.5:8.5), which possesses the largest amount of such species, delivers the

highest space-time yield of mixed alcohols - about three times that of the undoped Mo_2C catalyst - under the relatively mild conditions of 180 °C and 5 MPa.

In summary, Mo_2C-based catalysts show outstanding potential for syngas-to-alcohol synthesis through multidimensional modification and broad applicability. By synergistically regulating promoters (such as Ni, Rh, and K)[117,115] and strategically selecting supports with distinct properties (e.g., lignin-derived carbon and γ-Al_2O_3), these catalysts can be effectively tailored to diverse reaction scenarios. Constructing three-dimensional (3D) hierarchical porous structures offers a promising direction for further enhancing catalytic performance. Mechanistic studies of chlorinated volatile organic compound (CVOC) abatement reveal that the dissociation and activation of recalcitrant molecules are governed by surface acid-base and redox properties, with C-Cl bonds dissociating on Lewis acid sites and the resulting intermediates undergoing dehydrochlorination by hydroxyl species[118]. Moreover, catalytic steam reforming over β-Mo_2C/γ-Al_2O_3 converts refractory CVOC waste into syngas with a conversion efficiency above 95% at 600 °C[116], coupling pollutant removal with feedstock supply for alcohol synthesis and providing an innovative route for environmental remediation and carbon-resource recycling.

Rh-based catalyst

Among various catalysts for CO hydrogenation, Rh-based catalysts are considered highly promising for synthesizing C_2 oxygenates from syngas, owing to their unique capability. However, the commercial application of rhodium (Rh) is significantly constrained by its high cost as a noble metal[119,120]. While traditional homogeneous Rh-based catalysts exhibit high activity and selectivity, they pose challenges for product separation. Conversely, heterogeneous catalysts, though easily recoverable, often suffer from insufficient activity and selectivity due to low ligand concentrations and limited mobility of active sites[121]. These limitations can be mitigated by using supports with high specific surface area, hierarchical pore structures, and high nitrogen content[122]. Metal particle size is a critical parameter governing the performance of heterogeneous catalysts; typically, the specific atomic activity increases markedly as particle size decreases. When the metal particle size reaches the ultra-small limit, single-atom catalysts (SACs) form[123,124].

Arevalo *et al.*[125] found that deep hydrogenation to produce methane readily occurs on stepped Rh surfaces; therefore, modification and promoter tuning are required to modulate the kinetic competition between CH_x hydrogenation and CO insertion. Figure 6A illustrates the full reaction pathway for higher alcohol synthesis from syngas on stepped Rh (211) surfaces. The reaction is initiated by CO hydrogenation to form CHO (Formyl), from which multiple competing reaction branches diverge. The CHO intermediate can be hydrogenated to methanol or undergo dehydroxylation to yield CH_x species. C_1 fragments react with CO/CHO via insertion to form ethanol; ethanol can further undergo dehydroxylation to generate ethyl species, which sequentially produce n-propanol. Continuous hydrogenation of CH_x species leads to methane formation. Colored arrows in the figure distinguish insertion, hydrogenation, dehydroxylation, and desorption processes, explicitly revealing the competitive mechanism that governs the formation of target alcohols and methane byproducts. Figure 6B presents catalyst structural models and density functional theory (DFT)-calculated Gibbs free energy profiles to compare the reaction energy barriers at high-coordination terrace sites of Rh (111) and low-coordination step sites of Rh (221)[126]. Theoretical calculations confirm that low-coordination Rh (221) step sites facilitate C-O bond cleavage and $^*CH_x$ hydrogenation, promoting the formation of a methane byproduct, while boron oxides can spontaneously and selectively anchor and block such step sites[127]. Conversely, high-coordination Rh (111) terrace sites favor the coupling of $^*CH_2$ with CO/*CHO to produce C_2 oxygenates[126]. Collectively, boron species shield active sites for methane formation and raise the energy barrier for C-O cleavage and hydrogenation while preserving sites for carbon chain coupling. This clarifies the intrinsic mechanism by which boron modification suppresses

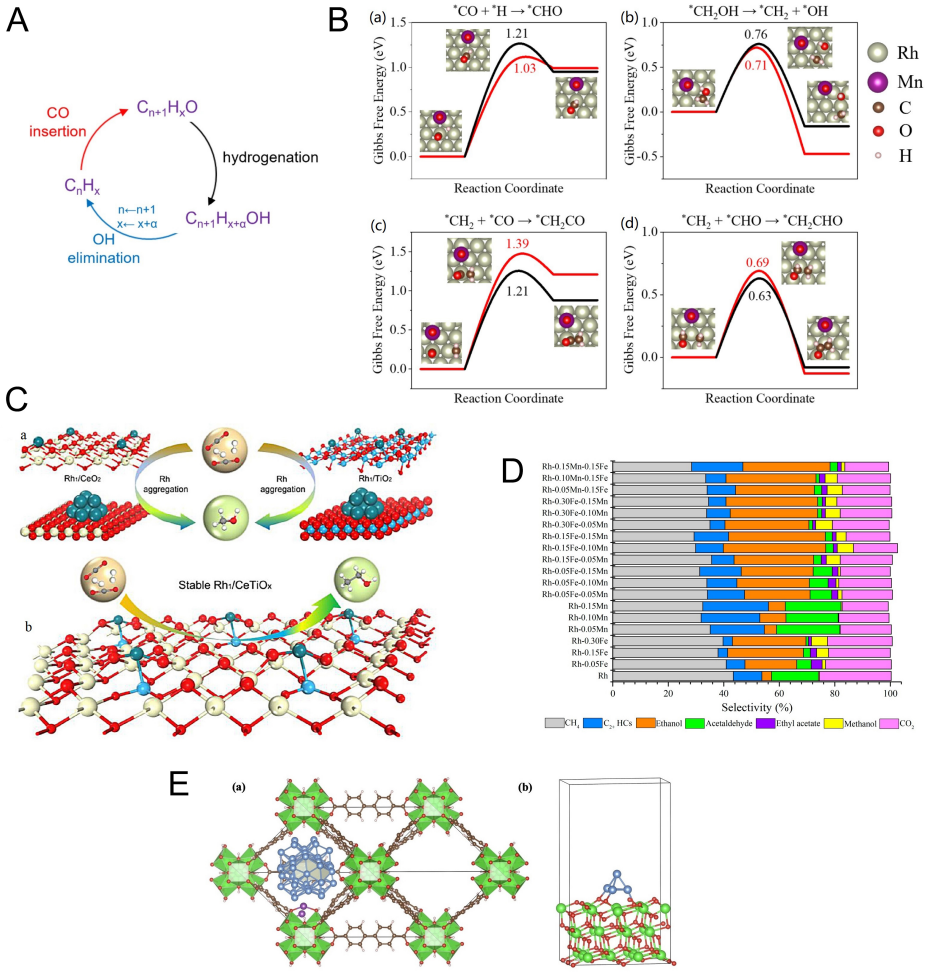

Figure 6. (A) The overall reaction cycle for HAS consisting of CO insertion (red), hydrogenation (black), and OH elimination (blue). (A) is reprinted with permission from Ref.[125], Copyright © 2024 Springer US; (B) (a-d) Gibbs free energy diagrams and configurations for four intermediate steps on Mn_1O_1 supported on the Rh (111) facet (black line) and (221) facet (red line) at 595 K. The insets in (a–d) show the configurations of the initial state (IS), transition state (TS) and final state (FS) on Rh (111). (B) is reprinted with permission from Ref.[126], Copyright © 2025 The Royal Society of Chemistry; (C) Schematic reaction process for long-term stability testing in CO_2 hydrogenation to ethanol over single-atom Rh supported on CeO_2, TiO_2 (a), and $CeTiO_x$ (b). (C) is reprinted with permission from Ref.[128], Copyright © 2022 WILEY; (D) Summary of selectivities for syngas conversion over Rh/SiO_2 and Rh-based multimetallic catalysts. (D) is reprinted with permission from Ref.[132], Copyright © 2017 American Chemical Society; (E) Optimized structures of Rh^+-Rh^0 /UiO-67 (a) and Rh^0/t-ZrO_2(101) (b). C, brown; O, red; H, white; Zr, green; Rh^+, purple; Rh0, blue; this color code is used throughout the paper. Details of model construction and charge analyses can be found in the Supporting Information. (E) is reprinted with permission from Ref.[135], Copyright © 2024 WILEY. HAS: higher-alcohol synthesis.

methane generation and boosts ethanol selectivity at the molecular scale.

Structural distortion facilitates the incorporation of Rh atoms and the formation of shorter Rh-O bonds [Figure 6C], while significantly increasing the aggregation energy barrier of Rh single-atom sites (Rh SASs)[128]. This confirms a strong interaction between Rh single atoms and surface O atoms, which endows the $Rh_1/CeTiO_x$ catalyst with exceptional structural stability, thereby ensuring high catalytic performance and outstanding long-term durability for ethanol production. Consequently, regulating support doping is pivotal for optimizing single-atom catalyst performance. Notably, maintaining a low Rh loading is crucial for achieving high ethanol selectivity. Conversely, high loading tends to induce Rh cluster formation, shifting the reaction pathway toward methanol or methane formation[129].

The active centers of SACs consist of isolated metal atoms, which provide single metal sites but cannot inherently form metal-metal bonds[130]. To address this limitation, Gong *et al.*[131] fabricated $RhFeO_x/TiO_2$ catalysts via drying and calcination treatments using P25 (anatase/rutile mixed-phase TiO_2) as the support, with iron introduced as a promoter. Benefiting from a fourfold synergistic effect, the Fe promoter constructs composite Rh^0-$Rh^{\delta+}$-O_v-Ti^{3+} active sites at the anatase-rutile phase boundaries of P25. Specifically, Fe generates abundant O_v-Ti^{3+} defects, synchronously regulates the coexistence of Rh^0 and $Rh^{\delta+}$ species, strengthens the SMSI at the phase junctions, and immobilizes ultrafine Rh nanoparticles at the anatase/rutile interfaces. This strategy addresses the inherent drawbacks of conventional single-atom catalysts and markedly accelerates the C-C coupling reaction.

Although introducing two promoters simultaneously can greatly improve overall selectivity toward oxygenates and C_2 hydrocarbons, systematic modulation of the deposition sequence and metal molar ratio is required; random doping weakens the synergistic effect. Figure 6D compares the carbon selectivity distribution of all products across monometallic Rh, binary Rh-Fe/Rh-Mn catalysts with different molar ratios, and ternary Rh-Fe-Mn catalysts prepared via varied deposition sequences[132]. Stepwise controllable surface deposition enables independent tuning of the surface coverage of Fe and Mn sites on Rh. Fe sites continuously convert acetaldehyde to ethanol, while Mn sites selectively facilitate C_2 olefin formation. Monometallic Rh mainly produces methane and acetaldehyde. Binary catalysts reduce methane selectivity and increase the proportion of ethanol or olefins, respectively. The ternary system simultaneously boosts the selectivity of ethanol and light hydrocarbons. Conversely, binary catalysts with a single promoter show competition between Fe and Mn for active sites on Rh, leading to a mutual offset of the two promoters' functions and only a limited reduction in methane selectivity[133].

Interface modulation between metal-support and metal-promoter interactions is a core strategy to tailor catalytic activity and product selectivity in CO_2 hydrogenation[134]. Figure 6E compares the atomic arrangement and charge distribution between the confined dual-site model of Rh^+-Rh^0/UiO-67 and the oxide-supported model of metallic Rh^0/t-ZrO_2(101)[135]. Rh dimers anchored inside UiO-67 cavities serve as Rh^+ sites, whereas intracavity Rh clusters act as Rh^0 sites with direct interfacial connections. Positively charged Rh^+ atoms construct a charge-differentiated dual active interface. Conversely, Rh nanoparticles on the t-ZrO_2 surface are nearly zero-valent metallic Rh, lacking cationic Rh sites and heterogeneous charge interfaces[136]. Bader charge analysis confirms that the metal-organic framework (MOF) framework modulates the charge distribution of Rh atoms to intrinsically generate adjacent Rh^+/Rh^0 sites. Oxide supports only immobilize homogeneous Rh clusters and cannot spontaneously form neighboring dual sites with separated valence states. Metal doping modification of Rh/ZrO_2 merely slightly adjusts the electron density of Rh, failing to reproduce the atomic-level valence-separated interface enabled by MOF confinement. Precise spatial confinement is a unique strategy for constructing charge-heterogeneous dual active sites.

In comparison with MOF-derived Cu/ZrO_2-DM catalysts for CO_2 hydrogenation to methanol, Cu-based catalysts enhance methanol yield by virtue of their large specific surface area and highly dispersed Cu active sites[137]. Conversely, Rh-based catalysts precisely manipulate reaction pathways via interfacial electronic effects. Together, these catalytic systems show that reactant adsorption and activation dictate product distribution, providing a theoretical framework for interfacial modulation in the rational design of catalysts for CO_2 hydrogenation to methanol and ethanol.

Multifunctional catalyst

In recent years, 85% of global energy and most chemical production have relied on fossil fuels. The resulting massive CO_2 emissions have significantly exacerbated global warming. This necessitates implementing technologies such as CO_2 capture[103] and utilization (CCU)[138,139] to achieve carbon cycling. Although

catalysts can significantly improve target-product yields, current transition-metal- and noble-metal-based catalysts suffer from critical limitations, including low ethanol yields and unsatisfactory selectivity. These challenges have prompted researchers to explore novel strategies for ethanol synthesis via CO_2 hydrogenation[140,141].

Figure 7A illustrates the tandem reaction pathway over solid Co FTS catalysts and molecular Co reductive hydroformylation (RHF) catalysts, whose performance is predominantly governed by the spatial distance between the two components[142]. When active sites are closely adjacent and molecular catalysts can diffuse into the pores of solid supports, the *in situ* formed 1-alkenes are rapidly trapped and converted into higher alcohols. Conversely, a large separation between active sites facilitates re-adsorption and hydrogenation of alkenes to paraffins, and only a small fraction of linear alcohols is produced directly via FTS[142]. Short inter-site distances reduce the diffusion path of alkene intermediates and suppress undesired saturation side reactions, thereby markedly boosting alcohol selectivity. Artificially isolating active sites leads to a substantial decline in alcohol yield. Although ligands enable fine-tuning of the linear-to-branched alcohol ratio, intimate synergism within confined pore channels is a prerequisite for efficient alcohol synthesis in this tandem system; simple physical mixing fails to deliver optimal catalytic performance. Accordingly, suitable spatial separation between the two components of bifunctional catalysts is critical to optimize intermediate migration, match reaction kinetics, and improve overall catalytic performance[143-145]. For supported Cu-based catalysts applied in ethanol conversion, an unbalanced spacing between Cu dehydrogenation sites and ZrO_2 acid sites impairs catalytic efficiency. Excessively large separation extends the diffusion pathway of reaction intermediates and accelerates side reactions, thereby lowering the selectivity toward ethyl acetate and substrate conversion. Conversely, an overly short distance causes metallic Cu to encapsulate zirconia acid sites, triggers sintering of Cu nanoparticles and deterioration of metal dispersion, and mismatches the reaction rates of dehydrogenation and condensation, ultimately hindering the formation of target products[146]. Figure 7B presents the Zr X-ray Photoelectron Spectroscopy (XPS) high-resolution spectra and the proportion of oxygen-deficient Zr^{x+} (Zr_1 species) over CuCoAl, CuCoAl|m-ZrO_2, and CuCoAl|t-ZrO_2 catalysts[147]. The composite system incorporating tetragonal ZrO_2 generates more oxygen-deficient Zr^{x+} sites, whereas fewer oxygen-deficient sites are formed in the monoclinic ZrO_2 composite system. Oxygen vacancies facilitate the water-gas shift reaction and stabilize oxygen-containing intermediates. The disparity in oxygen-deficient-site concentration directly governs CO_2 production and higher-alcohol selectivity. Accordingly, oxygen defects act as critical surface sites for modulating product distribution.

To address the challenges of low selectivity and insufficient stability in the conversion of syngas to ($C_{2+}OH$), Luan *et al.*[148] adopted a "reaction coupling strategy" to develop a bifunctional system composed of $ZnCrAlO_x$ (zinc-chromium-aluminum mixed oxide) and a K/Ni-promoted Mo-based sulfide (KNiMoS-MMO). Through component synergy, promoter modulation, and structural optimization, they achieved efficient conversion of syngas into low-carbon alcohols. Furthermore, leveraging proximity regulation, Lin *et al.*[149] engineered a catalyst comprising CoMn oxide and CuZnAlZr oxide. During extended operation, this catalyst maintained stable CO conversion rates, CO_2 selectivity, and product distribution (specifically the ratio of oxygenates to olefins) without significant deactivation, thereby satisfying the rigorous stability requirements for industrial applications [Figure 7C]. In another advancement, Jiang *et al.*[73] developed a multifunctional catalytic system centered on carbon matrix-encapsulated iron-based catalysts (Fe@NC) through a triple strategy involving precursor screening, K-promoter modification, and the co-addition of organic ligands. This design not only ensures efficient coupling between the RWGS and FTS reactions but also suppresses by-product formation, substantially improving selectivity toward long-chain hydrocarbons. Figure 7D compares the chemical states of surface carbon on catalysts modified by different alkali metals.

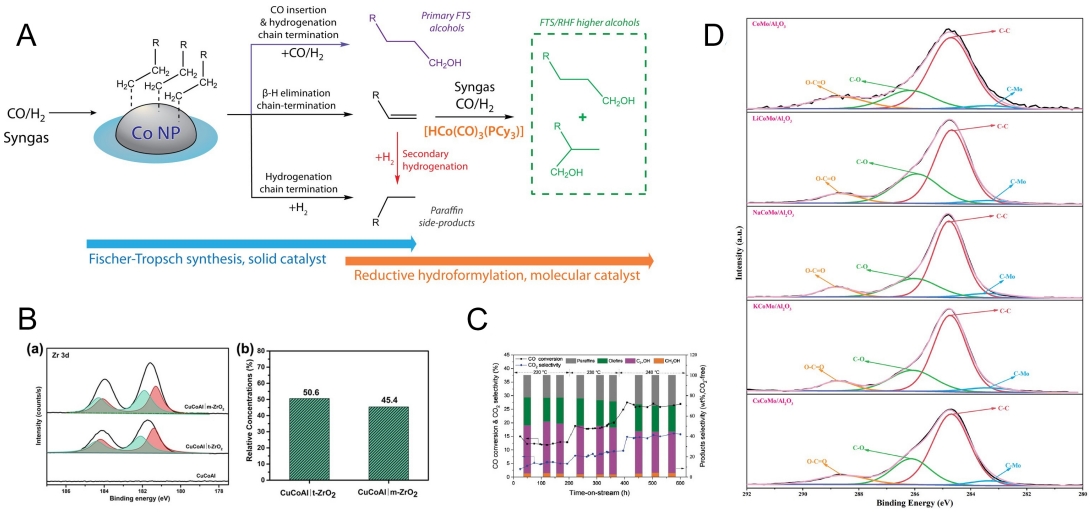

Figure 7. (A) Production of higher alcohols from syngas via the integration of Fischer-Tropsch synthesis (FTS) and reductive hydroformylation (RHF) in a tandem process. The active sites of the solid catalyst are responsible for chain growth (number of Cn in R). The ratio between β-H elimination and hydrogenation as chain termination steps determines the primary hydrocarbon selectivity, i.e., olefin-to-paraffin ratio. The activity of the molecular catalyst in olefin reductive hydroformylation relative to secondary olefin hydrogenation pathways determines the final alcohol selectivity. For completeness, the CO insertion chain-termination pathway on the FTS catalyst is also indicated as a source for primary, strictly linear higher alcohols. (A) is reprinted with permission from Ref.[142], Copyright © 2022 WILEY; (B) XPS spectra of CuCoAl, CuCoAljm-ZrO_2 and CuCoAljt-ZrO_2 catalysts after reduction. (a) Zr 3d, (b) The relative concentrations of Zrl species. (B) is reprinted with permission from Ref.[147], Copyright © 2021 John Wiley & Sons.; (C) Stability test of CoMn|CuZnAlZr multifunctional catalyst with mortar mixing. Reaction conditions: 6 MPa, H_2/CO = 2 and 2,000 mL/(g·h). (C) is reprinted with permission from Ref.[149], Copyright © 2019 WILEY; (D) C 1s spectrum of catalyst MCoMo/Al_2O_3. (D) is reprinted with permission from Ref.[150], Copyright © 2025 WILEY. XPS: X-ray photoelectron spectroscopy.

Four types of carbon characteristic peaks, namely graphitic carbon, C-Mo bonds, C-O, and C=O, can be fitted for all samples[150]. The C-Mo peak verifies the stable existence of the molybdenum carbide phase. Doping with Li, Na, K, and Cs does not alter the category of carbon species but only slightly adjusts the relative intensity of each carbon peak; the electronic effect of alkali metals exerts negligible influence on the surface carbon skeleton structure of catalysts. Compared with the unmodified catalyst, the proportion of oxygen-containing impurity carbon species in alkali-modified samples shows no obvious variation, and the peak position of the C-Mo characteristic peak remains nearly unchanged[151]. This indicates that alkali metals cannot directly regulate the electronic structure of molybdenum carbide, and the carbon carrier acts merely as a skeleton without modulating Mo valence states. Although alkali metals can tune metallic Mo active sites, they do not change the distribution of surface carbon species. Hence, carbon spectra cannot be adopted to screen the optimal promoters for alcohol synthesis. Overall catalytic performance is synergistically governed by multiple intrinsic preparation parameters, including fabrication procedures, thermal treatment temperature, and the physicochemical properties of carbon supports. Specifically, the nitrogen doping level, degree of graphitization, and porous structure of carbon supports can efficiently modulate electron-transfer efficiency and reactant mass-transport rates within the catalytic system.

In summary, multifunctional catalyst design does not follow a single, fixed paradigm. Instead, catalytic systems with target performance can be constructed by precisely combining and structurally regulating multiple components tailored to specific reaction requirements. Nevertheless, moderate proximity is imperative to achieve efficient synergy among various active sites.

INFLUENCING FACTORS

Preparation method

Currently, research on the catalytic hydrogenation of carbon dioxide to methanol has gradually focused on developing novel catalysts that are low-cost, environmentally friendly, and highly active. By regulating the interfacial contact between active metals and supports, as well as metal-support strong interactions, catalyst preparation protocols can simultaneously modulate the dispersion, reducibility, surface electronic structure of active components, and the adsorption-dissociation capacity of reactants. Meanwhile, these strategies enable precise control over the amount of target active phases formed during the reaction and improve catalyst sintering resistance[152]. Originating from the intrinsic physicochemical properties of catalysts, these approaches ultimately achieve simultaneous optimization of catalytic activity, methanol selectivity, and long-term operational stability. Accordingly, precise tuning of key physicochemical parameters (e.g., crystallite size, oxygen vacancy concentration, and the proportion of high-valence active species) via customized preparation strategies can systematically enhance the overall catalytic efficiency of CO_2 hydrogenation to methanol[153-154]. Table 5 systematically compares the core characteristics of four conventional catalyst synthesis routes, namely co-precipitation, ammonia evaporation, impregnation, and hydrothermal method, and summarizes the merits, drawbacks, and optimal applicable reaction domains of each technique. Precise modulation of catalytic performance can be achieved via these versatile synthetic strategies[164]. Based on practical reaction requirements, researchers can rationally select or further modify synthetic protocols to maximize advantages and mitigate deficiencies. Catalyst physicochemical properties can be optimized along multiple dimensions, including metal dispersion, pore structure, and metal-support interaction, thereby accommodating the distinct demands of diverse catalytic reactions in terms of activity, selectivity, and stability. For example, metal-organic frameworks (MOFs) are commonly prepared via six routes: solvothermal synthesis, microwave-assisted synthesis, direct pyrolysis, the sacrificial template method, post-synthetic modification, and supercritical fluid deposition (SFD). Comparative analyses reveal that MOFs prepared via these distinct methods have unique advantages, making them suitable for specific applications[53]. Similarly, San *et al.*[165] investigated Cu/ZrO_2 catalysts synthesized through four different methods and reached the same conclusion. Notably, compared with catalysts prepared by traditional methods, the Cu/ZrO_2-DM catalyst - synthesized via ligand replacement (partial substitution of terephthalic acid with amino terephthalic acid) combined with incipient wetness impregnation for Cu loading - exhibits superior catalytic performance[165]. In the broader context of catalyst optimization, refining preparation methods remains a pivotal approach to enhancing overall efficacy. By precisely regulating process parameters (e.g., reaction temperature, precursor ratios, and post-treatment conditions), the morphological structure, active site distribution, and electronic properties of catalysts can be optimized, thereby significantly improving their catalytic activity, selectivity, and stability[153].

Catalyst supports

Catalytic performance can be significantly enhanced through synergistic elemental interactions, optimized structural design, and strategic selection of supporting materials[166]. Metal supports play a multifaceted role in catalysis: they regulate the dispersion and valence state of active components to optimize active site architecture; facilitate reactant adsorption, activation, and intermediate transformation to streamline reaction pathways; strengthen metal-support interactions to bolster stability; and fine-tune pore structures and surface acid-base properties to improve mass transfer and selectivity[94,104,167-169]. Collectively, these effects synergistically elevate catalytic activity, selectivity, and durability. Carbon modification, a widely adopted support engineering strategy, effectively promotes the generation of surface oxygen vacancies, thereby strengthening CO_2 adsorption and activation. More importantly, carbon species intimately bound to metal components serve as efficient channels for hydrogen spillover. This saturates surface hydrogen adsorption and renders the H_2 reaction order near zero, effectively overcoming the kinetic limitations inherent in CO_2 hydrogenation to methanol[170]. Given the positive linear correlation between total alcohol selectivity and

Table 5. Comparison of core properties of Co-precipitation, ammonia evaporation, impregnation and hydrothermal methods

Evaluation index	Impregnation (conventional wet impregnation/methanol-assisted impregnation, e.g., Ni/KIT-6, NiMo/AC)	Ammonia evaporation (for metal loading on carbon/oxide supports)	Co-precipitation (Co-, Ni-, CuZnAl multi-metal systems)	Hydrothermal (*in situ* encapsulation & crystallization, NiMo@CNT, MOR zeolite)
References	[155,156]	[157-159]	[160,161]	[162,163]
Metal dispersion	Moderate to poor; metal precursors tend to agglomerate with large particle sizes (15-20 nm for Ni/SiO_2). Methanol modification and confined supports slightly improve dispersion	Excellent; ammonia complexes metal ions for uniform slow deposition, narrow particle size distribution; high dispersion for mono/bimetallic catalysts	Superior dispersion for multi-metals, poor for single metals. Simultaneous precipitation realizes atomic mixing of diverse metals, yet large aggregates and grain coarsening emerge after calcination	Excellent, controllable particle size (10-20 nm). Slow hydrothermal crystallization and *in situ* confinement suppress metal migration and agglomeration
Pore structure regulation	Metal particles easily block original support pores; BET surface area and pore volume drop sharply (733 → 497 m^2/g for KIT-6 after impregnation); broad pore size distribution	Slight pore blockage; thin uniform metal layer coats pore walls, preserving intrinsic support texture with narrow pore distribution	Abundant mesopores in precipitates, yet severe pore collapse upon calcination, disordered pores and lost micropores; poor repeatability even with precipitant adjustment	Ordered mesopores (KIT-6, CNT, zeolites) can be precisely tailored; tubular/cage confined structures are maintained for efficient mass transfer
Metal-support interaction	Weak, dominated by physical adsorption; low reduction temperature (372 °C for Ni/SiO_2), limited electron transfer and poor sintering resistance	Moderately strong; chemical bonding forms between metal and support hydroxyl groups with tunable electronic properties	Strong multi-interfacial interactions between metals and metal-oxides via co-crystallization, though bulky composite oxides readily form	Extremely strong dual effect of confinement and chemical bonding; directional electron transfer (Mo → Ni) generates abundant oxygen vacancies for enhanced activation
Advantages	Simple operation, low equipment cost, wide precursor range, accurate metal loading control, suitable for large-scale production	Optimal metal dispersion, compatible with carbon/SiO_2/Al_2O_3 supports, narrow particle size, good repeatability	One-step synthesis of multi-metal composites, low cost, easy scale-up, abundant multi-metal synergistic interfaces	Precise control over catalyst structure and defects; accessible *in situ* metal encapsulation, tunable acidity for N-doped carbon/zeolites
Disadvantages	Severe metal sintering at high temperatures, blocked pores increase mass transfer resistance, mediocre cycling stability	Long preparation cycle (12-24 h ammonia volatilization); local agglomeration at high metal loadings	High pH sensitivity, inconsistent batch performance, residual inorganic impurities, irreversible pore collapse after calcination	High cost of high-pressure reactors, low single-batch yield, difficult industrial scale-up, sensitive to temperature/pH/time
Cost&Scalability	Lowest cost, fully mature industrial technique	Medium cost, widely used in labs, limited to pilot trials	Low cost; mainstream industrial route for CuZnAl methanol/DME catalysts	Highest cost, only lab-scale small-batch synthesis

AC: Activated carbon; CNT: carbon nanotubes; MOR: mordenite; BET: brunauer-emmett-teller; DME: dimethyl ether.

oxygen vacancy concentration, increasing the density of surface oxygen vacancies is a proven approach to enhance total alcohol selectivity[171]. For example, in comparative studies of monometallic (Pt, Ni, Co) and bimetallic (PtNi, PtCo, PdNi) catalysts supported on CeO_2 (a reducible support) versus γ-Al_2O_3 (an irreducible support), the support type was found to primarily dictate catalytic activity and the extent of bimetallic bond formation[172]. As a representative reducible support, the morphology of CeO_2 directly influences oxygen vacancy concentration as well as the dispersion and stability of active metal species. Furthermore, particle size, modulated by calcination temperature, alters metal-support interactions and ultimately determines overall catalytic performance. Notably, CeO_2 can stabilize Rh in the +2 oxidation state, enabling efficient conversion of CO_2 to methane[173,174]. Conversely, irreducible supports like γ-Al_2O_3 generally

exhibit lower intrinsic activity but favor higher CO selectivity. Loading metals onto γ-Al_2O_3 also modifies the catalyst's basicity, yielding greater energy efficiency for syngas conversion and product formation[175].

Although product selectivity in catalytic reactions is intrinsically governed by supported active metal components, supports act far beyond simple physical scaffolds. Instead, they participate deeply in catalytic cycles and modulate reaction behavior across multiple dimensions, as shown by the Cu-based modified methanol synthesis catalysts and noble-metal single-atom Rh catalytic systems discussed in the foregoing sections. Previous literature has systematically summarized four core mechanisms by which supports regulate catalytic processes: *in situ* generation of auxiliary active sites, stabilization of key adsorbed reaction intermediates, construction of metal-support interfaces with electronic synergies, and modulation of reaction kinetics for the conversion of reactants and intermediates[142]. Collectively, these four mechanisms alter the intrinsic catalytic properties of catalysts.

Taking the Cu/ZrO_2 catalytic system for CO_2 hydrogenation to methanol elaborated in earlier chapters as an example, multiple regulatory effects originating from the support directly determine CO_2 conversion activity, target methanol selectivity, and long-term operational stability. ZrO_2 possesses moderate Lewis acidity and outstanding high-temperature anti-sintering capacity, which can anchor Cu nanoparticles and preserve mesoporous pore structures, rendering it the most suitable support for this reaction system[176]. Furthermore, the distance between the catalyst-relevant periphery (CRP) regions on the support surface and Cu active particles must be precisely matched to generate interfacial synergy[177]. Mismatched particle spacing directly disrupts the kinetic balance between CO_2 activation and formate intermediate transformation, and only optimized spacing can maximize catalytic efficiency. Such interfacial synergy rules serve as a critical prerequisite for high-efficiency production of oxygenates via CO_2 hydrogenation.

Extending to the single-atom noble metal catalytic system for selective ethanol synthesis through CO_2 hydrogenation discussed previously, the Rh_1/$CeTiO_x$ catalyst with Ti-doped $CeTiO_x$ support further highlights the multi-functional regulatory capacity of supports[125]. This composite oxide support is not merely an inert substrate for immobilizing isolated Rh single atoms; rather, it comprehensively reconstructs the catalytic system via four coupled core effects: (1) reversible surface structural reconstruction of the support to create high-density oxygen vacancy defects; (2) generation of SMSI between the support and Rh single atoms to precisely tune the electronic states of active sites; (3) fabrication of bifunctional active centers relying on defect sites and doped heterogeneous interfaces; (4) lattice confinement effect to suppress the migration and agglomeration of Rh single atoms and significantly improve the thermal stability of catalysts. These multi-layer regulatory mechanisms jointly determine the electronic distribution, spatial configuration of active sites, and complete reaction pathway covering CO_2 activation and C-C coupling, ultimately governing the overall catalytic activity, ethanol selectivity, and long-cycle durability of catalysts. This also provides clear theoretical guidance for the rational design of supports for single-atom noble metal catalysts.

Promoter

Consistent studies show that the performance of reactions represented by higher-alcohol synthesis from syngas and RWGS largely depends on modulating the surface chemical properties of catalysts[178-180]. Introducing secondary-metal or alkali-metal promoters into Mo-based (molybdenum carbide or molybdenum sulfide) catalysts is an effective way to precisely regulate the chemical structure and electronic environment of active sites[181].

The conventional RWGS reaction typically operates at elevated temperatures (400-700 °C), which not only predisposes catalysts to deactivation but also requires complex heat-exchange systems. Conversely, at lower temperatures (< 600 °C) and high pressure, CO_2 hydrogenation tends to favor methane and methanol formation, resulting in extremely low CO selectivity. Therefore, there is a critical need to develop catalysts

with both high activity and selectivity, and this demand can be effectively met by modifying catalysts with metal promoters. The synergistic interaction between the two metals alters the binding energies of reactants and reaction intermediates, fundamentally influencing the reaction's chemical behavior[182-184].

Alkali metal K represents the most widely adopted modifier/promoter in catalytic systems for higher alcohol synthesis from syngas. In recent years, K has emerged as a core tuning strategy to optimize catalytic activity, C_{2+} alcohol selectivity, and long-term operational stability by precisely modulating the electronic environment of active sites, surface defects, and reactant adsorption configurations[185]. It is compatible with various mainstream catalytic systems, including Mo-based catalysts and bimetallic Cu-Fe catalysts, providing an efficient regulatory route to overcome the intrinsic performance bottlenecks of different catalyst families.

As summarized from the foregoing comparative investigations of MoS_2 and Mo_2C molybdenum-based catalysts, under identical K and Mo loadings, MoS_2 sulfide catalysts construct abundant interlayer sulfur vacancies and heterogeneous MoS_2/$KMoS_2$ interfaces[104], which substantially strengthen CO insertion and C-C coupling kinetics. Accordingly, MoS_2 delivers superior C_{2+} alcohol selectivity and space-time yield relative to Mo_2C carbides. Conversely, the intrinsic active sites of Mo_2C favor the single-carbon hydrogenation pathway, yielding methanol and light alkanes as dominant products accompanied by abundant surface acidic sites[106]. Standard K doping dosages fail to deliver satisfactory regulation effects for Mo_2C; higher K loadings are therefore required to neutralize surface acidic sites, restructure CO adsorption modes, and ultimately elevate the fractions of total alcohols and long-chain alcohols in product distribution.

For the Mo_2C/γ-Al_2O_3 catalytic system described in previous sections, single-K modification improves the crystallinity of the β-Mo_2C phase and optimizes the valence distribution of Mo species[91]. When combined with Ni to form a dual-promoter system, K and Ni generate synergistic electronic effects that simultaneously tune the non-dissociative CO adsorption strength and balance the competing reactions of carbon chain propagation and hydrogenation. This suppresses excessive C-O bond hydrogenolysis from a kinetic perspective, mitigates the formation of hydrocarbon byproducts such as methane, and markedly boosts the yield of liquid alcohol products.

Within the bimetallic Cu-Fe catalyst category belonging to modified Fischer-Tropsch systems discussed earlier, the K promoter exerts multiple regulatory functions. On one hand, K accelerates the RWGS reaction over catalyst surfaces, continuously supplying active CO intermediates. Conversely, it modulates the electron density at metal-metal interfaces to enhance linear CO adsorption while weakening bridged CO adsorption, thereby delicately balancing the two competing pathways of CO dissociative and non-dissociative activation. Meanwhile, K lowers the energy barrier for C-C coupling and inhibits over-activation of H_2, restraining alkylation side reactions at the source to reduce alkane and alkene byproducts and selectively enrich C_{2+} alcohols[186]. Such regulatory effects effectively alleviate the inherent drawbacks of Cu-Fe catalysts, including facile phase segregation and overly broad product distribution.

COMPARISON OF DIFFERENT CATALYSTS IN SYNGAS-TO-HIGHER-ALCOHOL SYNTHESIS

Based on the above-mentioned catalytic systems for syngas-to-higher-alcohol synthesis, Table 6 statistically evaluates modified Fischer-Tropsch catalysts, Cu-based methanol-synthesis catalysts, Mo-based catalysts, Rh single-atom catalysts, and multifunctional composite catalysts under varied operating conditions, covering optimal temperature, pressure, H_2/CO molar ratio, CO conversion, total alcohol selectivity, and C_2^+-alcohol fraction. Combined with the intrinsic active-site configuration, support microstructure, and promoter modulation strategy of each category, this comparative analysis dissects how bimetallic interfacial interactions, defect engineering, surface electronic modulation, and tandem-site coordination govern CO

activation, C-C coupling, carbon-chain propagation, and final product distribution during syngas hydrogenation. This review emphasizes the underlying working mechanism, inherent bottlenecks, and key inter-system differences among these catalyst classes.

Modified Fischer-Tropsch catalysts rely on bimetallic interfacial sites to mediate C-C coupling and carbon-chain propagation, delivering superior long-chain-building capability relative to other monometallic alternatives, which renders them promising for higher-alcohol production. Nevertheless, two intrinsic drawbacks limit their practical deployment: narrow allowable temperature-pressure windows and abundant competing side reactions, creating a performance trade-off in which high CO conversion and high higher-alcohol selectivity cannot be readily achieved simultaneously. By comparison, Cu-based methanol-synthesis catalysts activate CO and H_2 via metallic Cu sites under mild conditions with low energy input; however, they lack efficient sites for C-C coupling[79]. This mechanistic deficiency fundamentally limits their capacity to generate long-chain alcohols. Moreover, Cu sites are prone to thermal sintering at elevated temperatures, leading to more severe deactivation than observed for modified Fischer-Tropsch and Mo-based counterparts.

Distinguished by unique lattice and electronic structures, Mo-based catalysts exhibit strong tolerance to sulfur and other impurities, enabling direct processing of crude, sulfur-containing syngas feedstocks - a major practical advantage that Cu-based and Rh-based catalysts cannot match. Unfortunately, their intrinsic catalytic activity is generally low, which compels harsh high-temperature/high-pressure operation to attain reasonable CO conversion and thus increases process energy consumption. In sharp contrast, Rh single-atom catalysts leverage atomically dispersed Rh sites to precisely steer reaction pathways, achieving the highest C_{2+} alcohol selectivity among the surveyed systems while suppressing undesired side-product formation. The principal barriers for Rh single-atom catalysts stem from material and structural aspects: high precious-metal cost, facile migration/leaching of isolated Rh sites, and complex fabrication protocols, which greatly compromise structural durability and industrial scalability compared with earth-abundant Cu- and Mo-based catalysts.

Multifunctional composite catalysts are designed to offset the weaknesses of single-component systems. Through defect engineering, surface electronic tuning, and tandem-site coordination, they integrate the carbon-chain-growth merit of modified Fischer - Tropsch catalysts, the mild-operation feature of Cu-based catalysts, the anti-poisoning robustness of Mo-based catalysts, and the high-selectivity trait of Rh-based catalysts. Such multi-site synergy enables balanced activity, alcohol selectivity, and operational stability, along with much greater flexibility in tuning product distribution than monofunctional catalysts. Even so, composite systems face formidable practical hurdles: precise component matching, sophisticated interfacial-synergy control, and unsatisfactory long-term stability, all of which pose technical barriers to real-world implementation relative to well-established single-component catalysts.

Collectively, the key distinctions across these catalyst families stem from their active-site nature: monometallic-type catalysts operate on relatively fixed reaction pathways with pronounced trade-offs among activity, selectivity, and stability, whereas composite catalysts rely on multi-site tandem synergy to break these trade-offs but require elaborate material fabrication. In terms of operational-condition compatibility, modified Fischer-Tropsch and Mo-based catalysts are adapted to harsh high-T/high-P environments, whereas Cu-based and Rh single-atom catalysts prefer milder, low-energy-consumption reaction regimes. This cross-system comparison clarifies mechanistic origins, pros and cons, and core differentiators of representative catalytic platforms, furnishing rational theoretical guidance for structural design and targeted modification of advanced syngas-to-higher-alcohol catalysts, and facilitating performance optimization and industrial-relevant evaluation of state-of-the-art syngas-conversion technologies.

Table 6. Master performance table of catalyst systems

Catalyst System	Optimal temperature	Optimal pressure	H_2/CO feed ratio	CO conversion	Total alcohol selectivity	C_{2+} alcohol proportion in total alcohols	Optimal catalyst	References
Modified F-T Cu-Co-based catalysts	240 °C	40 bar (4 MPa)	1.5	11.0% (Co_4Cu_1)	30.8%	/	Co_4Cu_1	[64]
Modified F-T Cu-Fe-based catalysts	260 °C	40 bar (4 MPa)	2.0	27.3% (peak at 0.5 wt% K)	/	/	0.5 wt% K modified CuFeMnZnO	[72]
Modified methanol synthesis Cu/ZnO/ZrO_2	No unified temperature & pressure for the optimal formulation C3Z2Z5	/	/	CO_2 conversion follows a volcanic curve with maximum value	Highest methanol space-time yield	Almost no C_{2+} alcohols	C3Z2Z5 (ZnO:ZrO_2 mass ratio = 2:5)	[86]
MoS_2 molybdenum sulfide catalysts	300-340 °C	3-7 MPa	1-2	Moderate	High	High proportion of C_{3+} alcohols	K & Co co-doped MoS_2	[106]
Mo_2C molybdenum carbide supported on Al_2O_3	300 °C	3.0 MPa	2	7.2%	67.6%	56% (37% ethanol)	KNiMo_2C/Al_2O_3	[109]
Mo_2C molybdenum carbide supported on lignin carbon (LC)	380 °C	7.0 MPa	1	47.9%	57.9%	76.7% (50.9% ethanol)	Ni/K/Mo_2C@LC	[94]
Single-atom Rh noble metal catalysts	Low temperature range: 220-270 °C	1-3 MPa	2	Medium to high	Outstanding ethanol selectivity	Ethanol as the dominant product	Rh_1/CeTiOx, RhLi@SiO_2	[125]
RhK/Mo_2C composite catalysts	No exclusive temperature marked	1 MPa/3 MPa	/	9.9% (1 MPa)/20.2% (3 MPa)	44.4%/51.4%	85.6%/71.0%	RhK/Mo_2C	[115]
Multifunctional tandem CoMn-CuZnAlZr catalysts	220-240 °C	6 MPa	2	No obvious decay over long-term operation	High oxygenate selectivity	Stable product distribution	Composite of CoMn oxide & CuZnAlZr oxide	[149]
FeCo Alloy carbide/CuZnAl tandem catalyst	Working condition for CO_2 hydrogenation	/	/	High CO_2 conversion	High ethanol selectivity	Ethanol as the major product	$(Fe_{3/4}Co_{1/4})_5C_2$/CZA	[52]

F-T: Fischer-Tropsch synthesis.

CONCLUSION AND OUTLOOK

A multi-system collaborative research paradigm has been established for higher-alcohol synthesis from syngas, yet each catalyst category suffers from inherent drawbacks and limited modification options. Modified Cu-Co Fischer-Tropsch catalysts are prone to metal-phase segregation, a seesaw effect triggered by variations in the Cu/Co molar ratio, sintering, and carbon deposition. Cu-based catalysts derived from modified methanol synthesis systems readily undergo water-induced deactivation at high temperatures and exhibit mismatched active interfaces. Molybdenum-based catalysts require harsh temperature and pressure conditions, and single-alkali modification fails to balance catalytic activity and C_{2+} alcohol selectivity. Rhodium-based noble metal catalysts incur excessive material costs, while high Rh loadings facilitate the formation of methane byproducts. Multifunctional tandem catalysts face difficulties in precisely tuning the spatial distance between active components, resulting in unsatisfactory interfacial synergy efficiency.

Unlike conventional reviews that merely tabulate catalytic performance and isolate modification rules, this review offers unique, systematic insights. Centered on the integrated reaction network of CO/CO_2 hydrogenation, it compares and analyzes CO activation and C-C coupling mechanisms across five major catalyst families. This research systematically summarizes the regulatory boundaries of four synthetic routes, supports, and promoters in modulating defect vacancies and metal-support interactions, as well as in tuning product distribution. A comprehensive structure-performance correlation framework linking synthesis procedure, microscopic morphology, active sites, and catalytic behaviors is constructed, offering systematic guidance for the rational design of high-efficiency catalysts.

Building on these advancements, future research on converting syngas to higher alcohols should focus on achieving breakthroughs in the following directions:

(i) Deepen mechanistic insights and structure-performance relationships. Leveraging advanced characterization techniques, including DFT calculations and attenuated total reflection surface-enhanced infrared absorption spectroscopy (ATR-SEIRAS), is essential for accurately elucidating the formation mechanisms of active sites, the CO adsorption-activation-coupling pathways, and the specific roles of promoters. This will provide a robust theoretical foundation for the rational and directed design of catalysts.

(ii) Advance collaborative innovation and performance optimization of catalyst systems. By integrating the structural advantages of diverse catalyst systems, high-efficiency composite catalytic materials can be developed. Research should target critical challenges - such as enhancing the activity of Mo-based catalysts and controlling the cost of Rh-based systems - by exploring novel promoter combinations and structural modification strategies to further improve $C_{2+}OH$ selectivity and long-term catalytic stability.

(iii) Accelerate process scale-up and industrialization. To overcome bottlenecks in process scaling, efforts must focus on optimizing reactor design and reaction conditions to establish low-cost, energy-efficient production processes tailored to China's energy structure. Furthermore, in-depth studies of catalyst deactivation mechanisms and regeneration technologies are crucial for resolving key industrial issues, including coking and the loss of active components.

(iv) Broaden feedstock diversity and application scenarios. Aligned with the "dual carbon" goals, research should intensify efforts on the coupled conversion of CO_2 and syngas into higher alcohols. Developing flexible catalytic processes adaptable to multi-feedstock systems will promote the diversified application of higher alcohols as fuels and chemical intermediates, thereby contributing to the construction of a sustainable, low-carbon energy system.

DECLARATIONS

Authors' contributions

Data sourcing, collection, and original draft writing: Chen, G.; Mei, X.
Data sourcing: Mei, X.
Data analysis and interpretation: Guo, N.; Wang, Q.; Wang, T.; Song, X.
Editing and supervision: Chen, G.; Wang, Z.
All authors participated in preparing the manuscript.

Availability of data and materials

Not applicable.

AI and AI-assisted tools statement

Not applicable.

Financial support and sponsorship

This work was financially supported by the National Natural Science Foundation of China (22578100, 52276181), the Natural Science Foundation of Henan Province (252300421904), the Key Scientific Research Projects of Higher Education Institutions in Henan Province (25A610002), the High-level Talent Research Launch Fund of Henan University of Technology (2023BS104), and the National Key Research and Development Program of China (2023YFB4203605).

Conflicts of interest

All authors declared that there are no conflicts of interest.

Ethical approval and consent to participate

Not applicable.

Consent for publication

Not applicable.

Copyright

REFERENCES

1. Mallapaty, S. How China could be carbon neutral by mid-century. *Nature* **2020**, *586*, 482-3. DOI PubMed
2. Chia, S. R.; Nomanbhay, S.; Ong, M. Y.; Shamsuddin, A. H. B.; Chew, K. W.; Show, P. L. Renewable diesel as fossil fuel substitution in Malaysia: a review. *Fuel* **2022**, *314*, 123137. DOI
3. Xu, X.; Zhou, Q.; Yu, D. The future of hydrogen energy: bio-hydrogen production technology. *Int. J. Hydrogen. Energy.* **2022**, *47*, 33677-98. DOI
4. Gumber, S.; Gurumoorthy, A. V. Methanol economy versus hydrogen economy. In *Methanol*; Elsevier, 2018; pp 661-74. DOI
5. Shindell, D.; Smith, C. J. Climate and air-quality benefits of a realistic phase-out of fossil fuels. *Nature* **2019**, *573*, 408-11. DOI PubMed
6. Chi, Y.; Zhang, Y.; Zhang, X.; Liu, B. Potential and health impact assessment of air pollutant emission reduction: a case study of China. *Clean. Techn. Environ. Policy.* **2025**, *27*, 1053-66. DOI
7. Pan, X.; Xu, J.; Wang, Y.; et al. A new perspective on hydrogenation of CO_2 into methanol over heterogeneous catalysts. *Prog. Nat. Sci. Mater. Int.* **2024**, *34*, 482-94. DOI
8. Weber, J. L.; Mejía, C. H.; de Jong, K. P.; de Jongh, P. E. Recent advances in bifunctional synthesis gas conversion to chemicals and fuels with a comparison to monofunctional processes. *Catal. Sci. Technol.* **2024**, *14*, 4799-842. DOI PubMed PMC
9. Man, Y.; Yang, S.; Qian, Y. Integrated process for synthetic natural gas production from coal and coke-oven gas with high energy efficiency and low emission. *Energy. Convers. Manag.* **2016**, *117*, 162-70. DOI
10. Granovskiy, M. Integrated coproduction of power and syngas from natural gas to abate greenhouse gas emissions without economic penalties. *ACS. Omega.* **2021**, *6*, 16336-42. DOI PubMed PMC
11. Yangbin, R.; Yujing, W.; Yiqing, Z.; Chao, H.; Yulong, Z.; Qi, S. Recent advances of Mo-based catalysts for synthesizing higher alcohols from syngas. *Mol. Catal.* **2024**, *568*, 114508. DOI
12. Cui, G.; Lou, Y.; Zhou, M.; Li, Y.; Jiang, G.; Xu, C. Review of mechanism investigations and catalyst developments for CO_2 hydrogenation to alcohols. *Catalysts* **2024**, *14*, 232. DOI
13. Zhang, Q.; Wang, S.; Dong, M.; Wang, J.; Fan, W. Recent advances in CO_2 hydrogenation to higher alcohols. *Sci. China. Chem.* **2025**, *68*, 2310-21. DOI
14. Xue, X.; Weng, Y.; Yang, S.; Meng, S.; Sun, Q.; Zhang, Y. Research progress of catalysts for synthesis of low-carbon alcohols from synthesis gas. *RSC. Adv.* **2021**, *11*, 6163-72. DOI PubMed PMC
15. Anekwe, I. M. S.; Nyembe, N.; Nqakala, L. C.; Madikizela, M.; Isa, Y. M. Sustainable fuels: lower alcohols perspective. *Environ. Prog. Sustain. Energy.* **2023**, *42*, e14175. DOI
16. Luk, H. T.; Mondelli, C.; Ferré, D. C.; Stewart, J. A.; Pérez-Ramírez, J. Status and prospects in higher alcohols synthesis from syngas. *Chem. Soc. Rev.* **2017**, *46*, 1358-426. DOI PubMed
17. Shown, B.; Gogoi, P.; Mitra, S.; Shown, I.; Bandyopadhyay, R.; Das, A. K. Emerging trends and future prospects of the catalytic conversion of syngas to higher alcohols. *ACS. Omega.* **2026**, *11*, 19963-20001. DOI PubMed PMC
18. Feng, J.; Badreldin, A.; Li, Y. Electrochemical CO_2 reduction to multicarbon fuels and chemicals: progress and prospects of tandem electrolyzer strategies. *Energy. Fuels.* **2025**, *39*, 21175-225. DOI PubMed PMC

19. Meng, W.; Jong, B. C. D.; Bovenkamp, H. V. D.; et al. Selectivity control between reverse water-gas shift and fischer-tropsch synthesis in carbon-supported iron-based catalysts for CO_2 hydrogenation. *Chem. Eng. J.* **2024**, *489*, 151166. DOI
20. Zhang, S.; Wu, Z.; Liu, X.; et al. Tuning the interaction between Na and Co_2C to promote selective CO_2 hydrogenation to ethanol. *Appl. Catal. B. Environ.* **2021**, *293*, 120207. DOI
21. Zhang, D.; Yang, W.; Wang, Z.; et al. Efficient electrochemical CO_2 reduction reaction on a robust perovskite type cathode with in-situ exsolved Fe-Ru alloy nanocatalysts. *Sep. Purif. Technol.* **2023**, *304*, 122287. DOI
22. Zhou, G.; Li, B.; Cheng, G.; et al. Concentrated C_{2+} alcohol production enabled by post-intermediate modulation and augmented CO adsorption in CO electrolysis. *J. Am. Chem. Soc.* **2024**, *146*, 31788-98. DOI
23. Hu, X.; Zhang, Z.; Li, Z.; et al. Stable Cu^{+}/Cu^{2+} species derived from in-situ growing Cu-S-V bonds in CuV_xS electrocatalysts enables high efficiency CO_2 electroreduction to methanol. *Appl. Catal. B. Environ. Energy.* **2024**, *358*, 124445. DOI
24. Kang, K.; Sampei, H.; Sekine, Y. CO_2 conversion to CO by reverse water gas shift and dry reforming using chemical looping. *RSC. Sustain.* **2025**, *3*, 1598-628. DOI
25. Zhang, B.; Huang, S.; Li, Y.; Shen, J.; Tian, X.; Ding, M. Highly dispersed Cu on hollow spherical CeO_2: an efficient and stable catalyst for the RWGS reaction. *Appl. Catal. B. Environ. Energy.* **2025**, *366*, 125003. DOI
26. Xu, Y.; Zhang, Z.; Wu, K.; et al. Effects of surface hydrophobization on the phase evolution behavior of iron-based catalyst during Fischer-Tropsch synthesis. *Nat. Commun.* **2024**, *15*, 7099. DOI
27. Xu, Y.; Ding, M. Development of hydrophobic catalysts for reducing the CO_2 emission during the conversion of syngas into chemicals and fuels. *Chem. Soc. Rev.* **2025**, *54*, 2881-905. DOI PubMed
28. Abd Aziz, A. J.; Baharuddin, N. A.; Somalu, M. R.; Muchtar, A. Layering optimization of the $SrFe_{0.9}Ti_{0.1}O_{3-\delta}$-$Ce_{0.8}Sm_{0.2}O_{1.9}$ composite cathode. *Molecules* **2022**, *27*, 2549. DOI PubMed PMC
29. Chung, C.; Tu, F.; Chiu, T.; Wu, T.; Yu, W. Critical roles of surface oxygen vacancy in heterogeneous catalysis over ceria-based materials: a selected review. *Chem. Lett.* **2021**, *50*, 856-65. DOI
30. Masters, C. The Fischer-Tropsch reaction. In *Advances in Organometallic Chemistry*; Catalysis and Organic Syntheses, Vol. 17; Elsevier, 1979; pp 61-103. DOI
31. Davis, B. H. Fischer-Tropsch synthesis: overview of reactor development and future potentialities. *Top. Catal.* **2005**, *32*, 143-68. DOI
32. Surisettya, V. R.; Dalai, A. K.; Kozinski, J. Alcohols as alternative fuels: an overview. *Appl. Catal. A. Gen.* **2011**, *404*, 1-11. DOI
33. Kabwe, F. B.; Jiang, Q.; Wang, C. Interfacial active sites in catalysts for higher alcohol synthesis from CO_2: a review. *Chemistry* **2026**, e71373. DOI PubMed
34. Wang, L.; Templer, R.; Murphy, R. J. Environmental sustainability of bioethanol production from waste papers: sensitivity to the system boundary. *Energy. Environ. Sci.* **2012**, *5*, 8281. DOI
35. Liu, K.; Atiyeh, H. K.; Tanner, R. S.; Wilkins, M. R.; Huhnke, R. L. Fermentative production of ethanol from syngas using novel moderately alkaliphilic strains of Alkalibaculum bacchi. *Bioresour. Technol.* **2012**, *104*, 336-41. DOI PubMed
36. Kang, J.; He, S.; Zhou, W.; et al. Single-pass transformation of syngas into ethanol with high selectivity by triple tandem catalysis. *Nat. Commun.* **2020**, *11*, 827. DOI PubMed PMC
37. Liu, G.; Yang, G.; Peng, X.; Wu, J.; Tsubaki, N. Recent advances in the routes and catalysts for ethanol synthesis from syngas. *Chem. Soc. Rev.* **2022**, *51*, 5606-59. DOI
38. Rommens, K. T.; Saeys, M. Molecular views on Fischer-Tropsch synthesis. *Chem. Rev.* **2023**, *123*, 5798-858. DOI PubMed
39. Schulz, H. Short history and present trends of Fischer-Tropsch synthesis. *Appl. Catal. A. Gen.* **1999**, *186*, 3-12. DOI
40. Platero, F.; Todorova, S.; Aoudjera, L.; et al. Cobalt stabilization through mesopore confinement on TiO_2 support for Fischer-Tropsch reaction. *ACS. Appl. Energy. Mater.* **2023**, *6*, 9475-86. DOI
41. Yang, Y.; Yu, F.; Ding, D.; et al. Effect of the Nd promoter on precipitated iron-based catalysts for high-temperature Fischer-Tropsch synthesis of light olefins. *RSC. Adv.* **2026**, *16*, 29712-21. DOI
42. Zhao, Y.; Wu, D.; Long, C.; et al. Engineering support surface to form metal alloy via atom migration for efficient CO hydrogenation. *ACS. Catal.* **2025**, *15*, 16165-75. DOI
43. Lindley, M.; Stishenko, P.; Crawley, J. W. M.; et al. Tuning the size of TiO_2-supported Co nanoparticle Fischer-Tropsch catalysts using Mn additions. *ACS. Catal.* **2024**, *14*, 10648-57. DOI
44. Cao, B.; Li, F.; Han, S.; Xu, Q.; Gu, J. Electrocatalytic CO reduction to produce long-chain products through Fischer-Tropsch pathway. *ChemElectroChem* **2025**, *12*, e202400595. DOI
45. Santos-carballal, D.; Cadi-essadek, A.; de Leeuw, N. H. Catalytic conversion of CO and H_2 into hydrocarbons on the cobalt Co(111) surface: implications for the Fischer-Tropsch process. *J. Phys. Chem. C.* **2021**, *125*, 11891-903. DOI

46. Chen, Y.; Wei, J.; Duyar, M. S.; Ordomsky, V. V.; Khodakov, A. Y.; Liu, J. Carbon-based catalysts for Fischer-Tropsch synthesis. *Chem. Soc. Rev.* **2021**, *50*, 2337-66. DOI
47. Rofer-depoorter, C. K. A comprehensive mechanism for the Fischer-Tropsch synthesis. *Chem. Rev.* **1981**, *81*, 447-74. DOI
48. Liu, J.; Wang, P.; Xu, W.; Hensen, E. J. Particle size and crystal phase effects in Fischer-Tropsch catalysts. *Engineering* **2017**, *3*, 467-76. DOI
49. Fan, Z.; Li, Z.; Li, Y.; et al. Boosting selectivity toward long-chain α-olefins in CO_2 hydrogenation through strengthening ZnO-Fe interactions with favorable iron phase regulation for Fischer-Tropsch synthesis. *JACS. Au.* **2026**, *6*, 1702-17. DOI
50. Moulay, I.; Hossain, M. M. CO_2 to sustainable aviation fuel via RWGS and Fischer-Tropsch: a comprehensive review on catalysts, kinetics, and reactor design. *Mol. Catal.* **2026**, *596*, 115881. DOI
51. Azancot, L.; Tarifa, P.; Cazaña, F.; Monzón, A. Fe-based catalysts on cellulose-derived carbon towards low-temperature RWGS. *Biomass. Bioenergy.* **2025**, *199*, 107894. DOI
52. Wang, W.; Guo, X.; Wang, Y.; et al. Transformation of CO_2 to C_{2+} alcohols by tailoring the oxygen bonding via Fe-based tandem catalyst. *Nat. Commun.* **2025**, *16*, 7265. DOI PubMed PMC
53. Ding, J.; Liu, Q.; Ye, R.; et al. Metal-support interactions in Fe-Cu-K admixed with SAPO-34 catalysts for highly selective transformation of CO_2 and H_2 into lower olefins. *J. Mater. Chem. A.* **2021**, *9*, 21877-87. DOI
54. Rabee, A. I. M.; Abed, H.; Vuong, T. H.; et al. CeO_2-supported single-atom Cu catalysts modified with Fe for RWGS reaction: deciphering the role of Fe in the reaction mechanism by in situ/operando spectroscopic techniques. *ACS. Catal.* **2024**, *14*, 10913-27. DOI
55. Zubkov, I. N.; Denisov, O. D.; Timokhina, M. A.; Savostyanov, A. P.; Yakovenko, R. Studying of the effect of gas recycle ratio on the formation of C5-C18 alkenes in the Fischer-Tropsch synthesis. *Catal. Ind.* **2024**, *16*, 443-50. DOI
56. Lu, Z.; Guo, L.; Shen, Q.; Bi, F.; Li, C.; Zhang, X. The application of metal-organic frameworks and their derivatives in the catalytic oxidation of typical gaseous pollutants: recent progress and perspective. *Sep. Purif. Technol.* **2024**, *340*, 126772. DOI
57. Zhao, F.; Zhang, C.; Guo, M.; et al. CO_2 hydrogenation to methanol over Ni/In_2O_3: effects of In_2O_3 morphology. *ACS. Catal.* **2025**, *15*, 18404-15. DOI
58. Wang, Z.; Cao, J.; Tang, W.; et al. Facile synthesis of low-cost Co-Cu/C alloy catalysts for hydrogen-rich syngas production from low-temperature steam reforming of biomass tar. *Chem. Eng. Sci.* **2023**, *267*, 118370. DOI
59. Yang, J.; Xue, D.; Geng, S.; et al. The role of hydroxyl groups on SiO_2 supported CuCo catalyst in the direct synthesis of ethanol from syngas. *Mol. Catal.* **2025**, *581*, 115147. DOI
60. de Reviere, A.; Verberckmoes, A.; Sabbe, M. K. Mechanistic origins for the enhanced ethanol dehydration kinetics in H-ZSM-5 by cofeeding *n*-butanol. *Catal. Sci. Technol.* **2024**, *14*, 4319-40. DOI
61. Xu, X.; Su, J.; Tian, P.; et al. First-principles study of C_2 oxygenates synthesis directly from syngas over CoCu Bimetallic catalysts. *J. Phys. Chem. C.* **2015**, *119*, 216-27. DOI
62. Telaar, P.; Schwiderowski, P.; Schmidt, S.; Stürmer, S.; Muhler, M. High-pressure CO, H_2, CO_2 and ethylene pulses applied in the hydrogenation of CO to higher alcohols over a bulk Co-Cu catalyst. *ChemCatChem* **2022**, *14*, e202200385. DOI
63. Sun, K.; Tan, M.; Bai, Y.; et al. Design and synthesis of spherical-platelike ternary copper-cobalt-manganese catalysts for direct conversion of syngas to ethanol and higher alcohols. *J. Catal.* **2019**, *378*, 1-16. DOI
64. Xiang, Y.; Barbosa, R.; Kruse, N. Higher alcohols through CO hydrogenation over CoCu catalysts: influence of precursor activation. *ACS. Catal.* **2014**, *4*, 2792-800. DOI
65. Mockenhaupt, B.; Özcan, F.; Dalebout, R.; et al. Cu-Co/$ZnAl_2O_4$ catalysts for CO conversion to higher alcohols synthesized from Co-precipitated hydrotalcite precursors. *Chem. Ing. Tech.* **2022**, *94*, 1784-97. DOI
66. Makgae, O. A.; Phaahlamohlaka, T. N.; Yao, B.; et al. Atomic structure and valence state of cobalt nanocrystals on carbon under syngas versus hydrogen reduction. *J. Phys. Chem. C.* **2022**, *126*, 6325-33. DOI
67. Sun, K.; Geng, S.; Liu, Z.; et al. Nitrogen-doped activated carbon supported CuCo catalysts with electronic synergy for highly efficient syngas conversion to ethanol. *Fuel* **2026**, *416*, 138590. DOI
68. Han, C.; Liu, J.; Li, L.; et al. Active sites on the CuCo catalyst in higher alcohol synthesis from syngas: a review. *Molecules* **2024**, *29*, 4855. DOI PubMed PMC
69. Chen, B.; Zhu, C.; Feng, H.; et al. Enhancing higher alcohols selectivity in CO_2 hydrogenation over FeCu catalysts via Mg modification. *Catal. Today.* **2026**, *463*, 115614. DOI
70. Yang, L.; Pastor-pérez, L.; Villora-pico, J. J.; et al. Highly active and selective multicomponent Fe-Cu/CeO_2-Al_2O_3 catalysts for CO_2 upgrading via RWGS: impact of Fe/Cu ratio. *ACS. Sustain. Chem. Eng.* **2021**, *9*, 12155-66. DOI
71. Liu, Y.; Ma, Y.; Pu, X.; et al. Influence of supports in CuFe-based catalysts for hydrogenation of CO_2 to ethanol. *Fuel* **2025**, *395*, 135192. DOI

72. Ding, M.; Tu, J.; Qiu, M.; Wang, T.; Ma, L.; Li, Y. Impact of potassium promoter on Cu-Fe based mixed alcohols synthesis catalyst. *Appl. Energy.* **2015**, *138*, 584-9. DOI
73. Jiang, S.; Yi, M.; Liu, Z.; Chowdhury, A. D. Tailored iron-based catalysts with carbon matrix for improved CO_2-modified Fischer-Tropsch synthesis. *Mater. Today. Chem.* **2025**, *46*, 102757. DOI
74. Xu, D.; Ding, M.; Hong, X.; Liu, G. Mechanistic aspects of the role of K promotion on Cu-Fe-based catalysts for higher alcohol synthesis from CO_2 hydrogenation. *ACS. Catal.* **2020**, *10*, 14516-26. DOI
75. Dedov, A. G.; Loktev, A. S.; Ermakov, E. V.; Bykov, M. A.; Sadovnikov, A. A.; Cherednichenko, K. A. Hydrotalcite-derived catalysts based on Al, Mg, and Ni hydroxides with untypical nickel loadings: effects of Ni loading on textural properties and catalytic performance in dry reforming of methane to syngas. *Pet. Chem.* **2025**, *65*, 778-87. DOI
76. Yang, Q.; Fedorova, E. A.; Cao, D.; et al. Understanding Mn-modulated restructuring of Fe-based catalysts for controlling selectivity in CO_2 hydrogenation to olefins. *Nat. Catal.* **2025**, *8*, 595-606. DOI
77. Bao, Z.; Ding, W.; Li, Q. Effect of Fe/Cu ratio on the activity of Fe-Al-Cu catalysts for water gas shift reaction under hydrogen-rich atmosphere. *Int. J. Hydrogen. Energy.* **2012**, *37*, 951-5. DOI
78. Smith, K. A chain growth scheme for the higher alcohols synthesis. *J. Catal.* **1984**, *85*, 428-36. DOI
79. Gao, P.; Zhang, L.; Li, S.; Zhou, Z.; Sun, Y. Novel heterogeneous catalysts for CO_2 hydrogenation to liquid fuels. *ACS. Cent. Sci.* **2020**, *6*, 1657-70. DOI
80. Tian, M.; Ma, E.; Tian, X.; Huang, W.; Li, S. Modulation of oxygen vacancies on Cu/ZnO by promoter for higher alcohol synthesis from syngas. *ChemistryOpen* **2026**, *15*, e70233. DOI PubMed PMC
81. Forzatti, P.; Tronconi, E.; Pasquon, I. Higher alcohol synthesis. *Catal. Rev.* **1991**, *33*, 109-68. DOI
82. Boniface, M.; Götsch, T.; Dong, J.; et al. Dynamics of a Cu/ZnO/Al_2O_3 catalyst revealed by operando transmission electron microscopy during CO_2 hydrogenation. *Nat. Catal.* **2026**, *9*, 404-13. DOI
83. He, Q.; Li, Z.; Li, D.; et al. Mg enhanced the performance of Cu/ZnO/ZrO_2 for CO_2 hydrogenation to methanol and the mechanism investigation. *Mol. Catal.* **2024**, *558*, 114008. DOI
84. Zu, H.; Wu, H.; Tian, J.; Li, A.; Wang, J. Unraveling the role of metal promoters (Zn, Cu, Co, Mn and Mg) in CO_2 hydrogenation to light olefins over Fe-K catalysts. *Mol. Catal.* **2025**, *580*, 115104. DOI
85. Singh, R.; Tripathi, K.; Pant, K. K.; Parikh, J. K. Unravelling synergetic interaction over tandem Cu-ZnO-ZrO_2/hierarchical ZSM5 catalyst for CO_2 hydrogenation to methanol and DME. *Fuel* **2022**, *318*, 123641. DOI
86. Chang, X.; Zi, X.; Li, J.; et al. An insight into synergistic metal-oxide interaction in CO_2 hydrogenation to methanol over Cu/ZnO/ZrO_2. *Catalysts* **2023**, *13*, 1337. DOI
87. Li, H.; Wang, L.; Gao, X.; Xiao, F. Cu/ZnO/Al_2O_3 catalyst modulated by zirconia with enhanced performance in CO_2 hydrogenation to methanol. *Ind. Eng. Chem. Res.* **2022**, *61*, 10446-54. DOI
88. Simanungkalit, S. P.; Okoye, C. O.; Zhang, Z.; Wu, J.; Zhang, D. Enhancing the catalytic performance of Cu/ZnO/Al_2O_3 catalyst in methanol synthesis from biomass-derived syngas with CeO_2, MnO_2 and ZrO_2 as promoters. *Asia-Pacific. J. Chem. Eng.* **2024**, *19*, e3121. DOI
89. López-Luque, I.; Hack, J.; Ródenas, T.; et al. Engineering peripheral metal-oxide catalysis: interparticle spacing in Cu/ZrO_2 catalysts for methanol synthesis by CO_2 hydrogenation. *Angew. Chem. Int. Ed.* **2025**, *64*, e202420126. DOI
90. Liakakou, E.; Heracleous, E.; Triantafyllidis, K.; Lemonidou, A. K-promoted NiMo catalysts supported on activated carbon for the hydrogenation reaction of CO to higher alcohols: effect of support and active metal. *Appl. Catal. B. Environ.* **2015**, *165*, 296-305. DOI
91. Spivey, J. J.; Egbebi, A. Heterogeneous catalytic synthesis of ethanol from biomass-derived syngas. *Chem. Soc. Rev.* **2007**, *36*, 1514-28. DOI PubMed
92. Maximov, V. V.; Permyakov, E. A.; Dorokhov, V. S.; Wang, A.; Kooyman, P. J.; Kogan, V. M. Effect of promoter nature on synthesis gas conversion to alcohols over (K)MeMoS$_2$/Al_2O_3 catalysts. *ChemCatChem* **2020**, *12*, 1443-52. DOI
93. Khusnutdinova, J. R.; Garg, J. A.; Milstein, D. Combining low-pressure CO_2 capture and hydrogenation to form methanol. *ACS. Catal.* **2015**, *5*, 2416-22. DOI
94. Meng, S.; Gu, J.; Jiang, S.; et al. Lignin carbon-initiated Ni/K/Mo_2C catalyst for efficient synthesis of higher alcohols from syngas. *Chem. Eng. J.* **2024**, *481*, 148751. DOI
95. Fang, K.; Li, D.; Lin, M.; Xiang, M.; Wei, W.; Sun, Y. A short review of heterogeneous catalytic process for mixed alcohols synthesis via syngas. *Catal. Today.* **2009**, *147*, 133-8. DOI
96. Rafique, M. U.; Cui, P.; Jia, W.; et al. Carbon-aerogel-confined MoO_2 as a robust nanocatalyst for the reverse water-gas shift reaction. *Nano. Lett.* **2026**, *26*, 3251-7. DOI

97. Sun, X.; Yu, J.; Zada, H.; et al. Reaction-induced unsaturated Mo oxycarbides afford highly active CO_2 conversion catalysts. *Nat. Chem.* **2024**, *16*, 2044-53. DOI
98. Zaman, S.; Smith, K. J. A Review of molybdenum catalysts for synthesis gas conversion to alcohols: catalysts, mechanisms and kinetics. *Catal. Rev.* **2012**, *54*, 41-132. DOI
99. Osman, M. E.; Konopatsky, A. S.; Repev, N. A.; Shtansky, D. V.; Nikulshin, P. A.; Kogan, V. M. Tuning ethanol synthesis pathways from syngas: nanosheet-structured K-doped Co-MoS_2 catalysts and the role of CVD sulfidation. *Catal. Sci. Technol.* **2025**, *15*, 3918-39. DOI
100. Zhou, S.; Ma, W.; Anjum, U.; et al. Strained few-layer MoS_2 with atomic copper and selectively exposed in-plane sulfur vacancies for CO_2 hydrogenation to methanol. *Nat. Commun.* **2023**, *14*, 5872. DOI PubMed PMC
101. Sun, X.; Yu, J.; Cao, S.; et al. In situ investigations on structural evolutions during the facile synthesis of cubic α-MoC_{1-x} catalysts. *J. Am. Chem. Soc.* **2022**, *144*, 22589-98. DOI
102. Wang, Q.; Li, X.; Ma, X.; Li, Z.; Yang, Y. Activation of the MoS_2 basal plane to enhance CO hydrogenation to methane activity through increasing S vacancies. *ACS. Appl. Mater. Interfaces.* **2022**, *14*, 7741-55. DOI
103. Zhao, T.; Shen, C.; Liu, Y.; et al. Bifunctional catalyst MoS_x@H-Beta for highly selective conversion of CO_2 to C_{2-6} hydrocarbons. *Catal. Sci. Technol.* **2024**, *14*, 2166-77. DOI
104. Zeng, F.; Xi, X.; Cao, H.; Pei, Y.; Heeres, H. J.; Palkovits, R. Synthesis of mixed alcohols with enhanced C3+ alcohol production by CO hydrogenation over potassium promoted molybdenum sulfide. *Appl. Catal. B. Environ.* **2019**, *246*, 232-41. DOI
105. Li, H.; Zhang, W.; Wang, Y.; et al. Nanosheet-structured K-Co-MoS_2 catalyst for the higher alcohol synthesis from syngas: synthesis and activation. *J. Energy. Chem.* **2019**, *30*, 57-62. DOI
106. Hu, J.; Wei, Z.; Zhang, Y.; et al. Edge-rich molybdenum disulfide tailors carbon-chain growth for selective hydrogenation of carbon monoxide to higher alcohols. *Nat. Commun.* **2023**, *14*, 6808. DOI PubMed PMC
107. Santos, V. P.; van der Linden, B.; Chojecki, A.; et al. Mechanistic insight into the synthesis of higher alcohols from syngas: the role of K promotion on MoS_2 catalysts. *ACS. Catal.* **2013**, *3*, 1634-7. DOI
108. Morrill, M. R.; Thao, N. T.; Agrawal, P. K.; et al. Mixed MgAl oxide supported potassium promoted molybdenum sulfide as a selective catalyst for higher alcohol synthesis from syngas: MoS_2/K_2CO_3 on mixed metal oxides for higher alcohol synthesis. *Catal. Lett.* **2012**, *142*, 875-81. DOI
109. Yang, Z.; Luo, M.; Liu, Q.; et al. Effect of K and Ni promoters on Mo_2C/Al_2O_3 catalyst for higher alcohols synthesis from syngas. *Kinet. Catal.* **2024**, *65*, 251-60. DOI
110. He, S.; Qu, H.; Liu, J.; et al. Remarkably enhanced catalytic performance of three-dimensional hierarchically porous Mo_2C catalysts for higher alcohols synthesis from syngas. *Mol. Catal.* **2024**, *556*, 113941. DOI
111. Hao, Z.; Li, X.; Tian, Y.; et al. Influence of carbon content in Ni-doped Mo_2C catalysts on CO hydrogenation to mixed alcohol. *Catalysts* **2021**, *11*, 230. DOI
112. Shou, H.; Ferrari, D.; Barton, D. G.; Jones, C. W.; Davis, R. J. Influence of passivation on the reactivity of unpromoted and Rb-promoted Mo_2C nanoparticles for CO hydrogenation. *ACS. Catal.* **2012**, *2*, 1408-16. DOI
113. Ahmadi Khoshooei, M.; Wang, X.; Vitale, G.; et al. An active, stable cubic molybdenum carbide catalyst for the high-temperature reverse water-gas shift reaction. *Science* **2024**, *384*, 540-6. DOI
114. Ren, M.; Chen, Y.; Feng, T.; et al. Methane dry reforming on N-doped carbon-supported Mo_2C catalysts: impacts of N functionality and Ni addition. *ChemCatChem* **2025**, *17*, e00541. DOI
115. Wang, C.; Yu, H.; Lin, T.; et al. Direct synthesis of higher alcohols from syngas over modified Mo_2C catalysts under mild reaction conditions. *Catal. Sci. Technol.* **2022**, *12*, 1697-708. DOI
116. Lin, F.; Chen, Z.; Gong, H.; Wang, X.; Qin, Y. Molybdenum carbide catalyst enables efficient conversion of chlorinated volatile organic waste into syngas through catalytic steam reforming. *ACS. Appl. Mater. Interfaces.* **2024**, *16*, 61868-76. DOI
117. Liakakou, E. T.; Heracleous, E. Transition metal promoted K/Mo_2C as efficient catalysts for CO hydrogenation to higher alcohols. *Catal. Sci. Technol.* **2016**, *6*, 1106-19. DOI
118. Zhang, L.; Deng, W.; Cai, Y.; Dai, Q.; Guo, L. Comparative studies of phosphate-modified CeO_2 and Al_2O_3 for mechanistic understanding of dichloromethane oxidation and chloromethane formation. *ACS. Catal.* **2020**, *10*, 13109-24. DOI
119. Yu, Z. K.; Jiang, M.; Dai, S.; Zhan, W.; Wang, Z. Q.; Gong, X. Q. Valence restrictive metal-support interaction for boosting catalytic activity of Rh/CeO_2 in CO_2 hydrogenation. *Nat. Commun.* **2025**, *16*, 9072. DOI PubMed PMC
120. Palomino, R. M.; Magee, J. W.; Llorca, J.; Senanayake, S. D.; White, M. G. The effect of Fe-Rh alloying on CO hydrogenation to C_{2+} oxygenates. *J. Catal.* **2015**, *329*, 87-94. DOI

121. Sun, Q.; Dai, Z.; Liu, X.; et al. Highly efficient heterogeneous hydroformylation over Rh-metalated porous organic polymers: synergistic effect of high ligand concentration and flexible framework. *J. Am. Chem. Soc.* **2015**, *137*, 5204-9. DOI
122. Ren, Z.; Liu, Y.; Lyu, Y.; et al. Single-atom Rh based bipyridine framework porous organic polymer: a high active and superb stable catalyst for heterogeneous methanol carbonylation. *J. Catal.* **2019**, *369*, 249-56. DOI
123. Yang, X. F.; Wang, A.; Qiao, B.; Li, J.; Liu, J.; Zhang, T. Single-atom catalysts: a new frontier in heterogeneous catalysis. *Acc. Chem. Res.* **2013**, *46*, 1740-8. DOI
124. Erdőhelyi, A. Hydrogenation of carbon dioxide on supported Rh catalysts. *Catalysts* **2020**, *10*, 155. DOI
125. Arevalo, R. L.; Nakanishi, H. A first principles mechanistic study of higher alcohol synthesis from syngas on a stepped rhodium surface. *Catal. Lett.* **2024**, *154*, 3418-25. DOI
126. Xiao, J.; Wang, C.; Meng, H.; et al. Spontaneous deposition of boron oxide on a rhodium nanostructure for selective conversion of syngas to ethanol. *Chem. Sci.* **2025**, *16*, 22002-9. DOI
127. Degerman, D.; Shipilin, M.; Lömker, P.; et al. Operando observation of oxygenated intermediates during CO hydrogenation on Rh single crystals. *J. Am. Chem. Soc.* **2022**, *144*, 7038-42. DOI PubMed PMC
128. Zheng, K.; Li, Y.; Liu, B.; Jiang, F.; Xu, Y.; Liu, X. Ti-doped CeO_2 stabilized single-atom rhodium catalyst for selective and stable CO_2 hydrogenation to ethanol. *Angew. Chem. Int. Ed.* **2022**, *61*, e202210991. DOI
129. Inoue, T.; Iizuka, T.; Tanabe, K. Hydrogenation of carbon dioxide and carbon monoxide over supported rhodium catalysts under 10 bar pressure. *Appl. Catal.* **1989**, *46*, 1-9. DOI
130. Peng, M.; Dong, C.; Gao, R.; Xiao, D.; Liu, H.; Ma, D. Fully exposed cluster catalyst (FECC): toward rich surface sites and full atom utilization efficiency. *ACS. Cent. Sci.* **2021**, *7*, 262-73. DOI PubMed PMC
131. Gong, C.; Wang, H.; Zhang, J.; et al. Construction of active Rh-TiO_x interfacial sites on $RhFeO_x$/P25 for highly efficient hydrogenation of CO_2 to ethanol. *ACS. Catal.* **2024**, *14*, 17582-97. DOI
132. Liu, Y.; Göeltl, F.; Ro, I.; et al. Synthesis gas conversion over Rh-based catalysts promoted by Fe and Mn. *ACS. Catalysis.* **2017**, *7*, 4550-63. DOI
133. Preikschas, P.; Bauer, J.; Knemeyer, K.; Naumann d'Alnoncourt, R.; Kraehnert, R.; Rosowski, F. Formation, dynamics, and long-term stability of Mn- and Fe-promoted Rh/SiO_2 catalysts in CO hydrogenation. *Catal. Sci. Technol.* **2021**, *11*, 5802-15. DOI
134. Liu, M.; Zou, R.; Yan, W.; et al. Dynamic restructuring of Rh/In_2O_{3-x} on ZrO_2 support for promoted selective hydrogenation of CO_2 to methanol. *ACS. Catal.* **2026**, *16*, 4463-75. DOI
135. Yu, J.; Liu, T.; Gu, Q.; et al. Enhanced proximity of Rh(1,2)-Rh(n) ensembles encaged in UiO-67 boosting catalytic conversion of syngas to oxygenates. *Angew. Chem. Int. Ed.* **2024**, *63*, e202401568. DOI
136. Li, S.; Feng, L.; Wang, H.; et al. Atomically intimate assembly of dual metal-oxide interfaces for tandem conversion of syngas to ethanol. *Nat. Nanotechnol.* **2025**, *20*, 255-64. DOI
137. Han, X.; Li, M.; Chang, X.; et al. Hollow structured Cu@ZrO_2 derived from Zr-MOF for selective hydrogenation of CO_2 to methanol. *J. Energy. Chem.* **2022**, *71*, 277-87. DOI
138. Kim, Y.; Lees, E. W.; Donde, C.; et al. Integrated CO_2 capture and conversion to form syngas. *Joule* **2024**, *8*, 3106-25. DOI
139. Sarmad, S.; Lu, D.; Gao, S.; et al. Advancing syngas production: a comparative techno-economic analysis of ICCU and CCU technologies for CO_2 emission reduction. *J. Environ. Chem. Eng.* **2024**, *12*, 114562. DOI
140. Corma, A. Preface to special issue of ChemSusChem on green carbon science: CO_2 capture and conversion. *ChemSusChem* **2020**, *13*, 6054-5. DOI
141. Solomon, S.; Plattner, G. K.; Knutti, R.; Friedlingstein, P. Irreversible climate change due to carbon dioxide emissions. *Proc. Natl. Acad. Sci. U. S. A.* **2009**, *106*, 1704-9. DOI PubMed PMC
142. Jeske, K.; Rösler, T.; Belleflamme, M.; et al. Direct conversion of syngas to higher alcohols via tandem integration of fischer-tropsch synthesis and reductive hydroformylation. *Angew. Chem. Int. Ed.* **2022**, *61*, e202201004. DOI
143. Xu, D.; Yang, H.; Hong, X.; Liu, G.; Edman Tsang, S. C. Tandem catalysis of direct CO_2 hydrogenation to higher alcohols. *ACS. Catal.* **2021**, *11*, 8978-84. DOI
144. Tan, K. B.; Zhan, G.; Sun, D.; Huang, J.; Li, Q. The development of bifunctional catalysts for carbon dioxide hydrogenation to hydrocarbons *via* the methanol route: from single component to integrated components. *J. Mater. Chem. A.* **2021**, *9*, 5197-231. DOI
145. Li, S.; Ma, Z.; Zhong, X.; et al. Hydrogen spillover-mediated spatial decoupling process boosts syngas conversion to higher oxygenates. *J. Am. Chem. Soc.* **2025**, *147*, 47187-202. DOI
146. Joshi, V. V.; Bollini, P. Exploiting proximity effects to improve ethyl acetate selectivity in the dehydrogenative coupling of ethanol over supported Cu catalysts. *Appl. Catal. A. Gen.* **2025**, *697*, 120228. DOI
147. Huang, C.; Zhu, C.; Zhang, M.; et al. Direct conversion of syngas to higher alcohols over a CuCoAl|t-ZrO_2 multifunctional catalyst. *ChemCatChem* **2021**, *13*, 3184-97. DOI

148. Luan, X.; Ren, Z.; Dai, X.; et al. Selective conversion of syngas into higher alcohols via a reaction-coupling strategy on multifunctional relay catalysts. *ACS. Catal.* **2020**, *10*, 2419-30. DOI
149. Lin, T.; Qi, X.; Wang, X.; et al. Direct production of higher oxygenates by syngas conversion over a multifunctional catalyst. *Angew. Chem. Int. Ed.* **2019**, *58*, 4627-31. DOI
150. Yang, Z.; Luo, M.; Liu, Q.; Rahman, R. Effect of alkali metals on $CoMo_2C/Al_2O_3$ catalysts for syngas to higher alcohols. *ChemCatChem* **2025**, *17*, e202402143. DOI
151. Yang, Z.; Luo, M.; Liu, Q.; et al. Effect of transition and alkali metals on Mo_2C/Al_2O_3 catalysts for syngas to higher alcohols. *J. Environ. Chem. Eng.* **2024**, *12*, 114455. DOI
152. Chen, M.; Cheng, C.; Wang, Q.; et al. Effects of preparation methods on Na-modified SiO_2-supported Fe catalysts for Fischer-Tropsch synthesis to light olefins. *React. Kinet. Mech. Catal.* **2026**, *139*, 1849-69. DOI
153. Liu, L.; Mezari, B.; Kosinov, N.; Hensen, E. J. M. Al promotion of In_2O_3 for CO_2 hydrogenation to methanol. *ACS. Catal.* **2023**, *13*, 15730-45. DOI PubMed PMC
154. Yang, M.; Yu, J.; Zimina, A.; et al. Unlocking a dual-channel pathway in CO_2 hydrogenation to methanol over single-site zirconium on amorphous silica. *Angew. Chem. Int. Ed.* **2024**, *63*, e202312292. DOI
155. Shen, W.; Zhang, X.; Huang, Y.; et al. Enhanced catalytic decomposition of methyl formate to carbon monoxide and methanol using palladium/activated carbon catalyst: mechanistic insights and catalyst design considerations. *Fuel* **2025**, *381*, 133099. DOI
156. Wei, Y.; Cai, W.; Deng, S.; et al. Efficient syngas production via dry reforming of renewable ethanol over Ni/KIT-6 nanocatalysts. *Renew. Energy.* **2020**, *145*, 1507-16. DOI
157. Zhou, Z.; Zhang, Y.; Wang, J.; et al. Synthesis of low-carbon alcohols from syngas over Cu-Fe/TiO_2 catalysts with an anatase-rutile junction. *ACS. Catal.* **2026**, *16*, 4961-71. DOI
158. Bukhtiyarova, M. V.; Bukhtiyarova, G. A. Highly dispersed Cu nanoparticles prepared using ammonia evaporation method. *ChemNanoMat* **2026**, *12*, e202500415. DOI
159. Fu, X.; Liu, Y.; Liu, Q.; Liu, Z.; Peng, Z. Preparation of highly active Cu/SiO_2 catalysts for furfural to 2-methylfuran by ammonia evaporation method. *Catalysts* **2022**, *12*, 276. DOI
160. Guzmán, H.; Roldán, D.; Sacco, A.; et al. CuZnAl-oxide nanopyramidal mesoporous materials for the electrocatalytic CO_2 reduction to syngas: tuning of H_2/CO ratio. *Nanomaterials* **2021**, *11*, 3052. DOI PubMed PMC
161. Hong, Z.; Wang, J.; Gao, Z.; Huang, W. Tuning CuO crystallite size by different solvents for higher alcohols synthesis from syngas over CuZnAl catalyst. *Int. J. Hydrogen. Energy.* **2024**, *56*, 1032-7. DOI
162. Zhang, Z.; Shen, Z.; Lin, X.; et al. In-situ synthesis of NiMo bimetallic nanoparticle encapsulated in carbon nanotubes for efficient and highly selective furfural hydrogenation. *J. Anal. Appl. Pyrolysis.* **2026**, *198*, 107883. DOI
163. Zhou, Y.; Yu, L.; Chang, J.; Feng, L.; Zhang, J. Low carbon alcohol fuel electrolysis of hydrogen generation catalyzed by a novel and effective Pt-CoTe/C bifunctional catalyst system. *Green. Energy. Environ.* **2024**, *9*, 758-70. DOI
164. Deng, G.; Tang, X.; Li, J.; Ling, S.; Yang, F.; Wang, S. The effect of catalyst preparation methods on biomass hydrothermal liquefaction: exploring cleaner and more efficient pathways for catalytic hydrothermal liquefaction of biomass. *Fuel* **2025**, *390*, 134709. DOI
165. San, X.; Li, X.; Zhang, L.; Meng, D.; Chang, X.; Qi, J. Highly dispersed active sites and strong metal-support interaction for boosting CO_2 hydrogenation to methanol. *Process. Saf. Environ. Prot.* **2024**, *187*, 320-31. DOI
166. Zhang, M.; Li, Y.; Tian, X.; et al. A review of iron-based catalysts for persulfate activation to remove PFAS in water: catalytic effects of various iron species, influencing factors and reaction pathways. *Water. Air. Soil. Pollut.* **2025**, *236*, 7632. DOI
167. Cheng, K.; Li, Y.; Kang, J.; Zhang, Q.; Wang, Y. Selectivity control by relay catalysis in CO and CO_2 hydrogenation to multicarbon compounds. *Acc. Chem. Res.* **2024**, *57*, 714-25. DOI
168. Tong, Y.; Xie, W.; Sun, H.; et al. Superior catalytic performance of Si-modified Al_2O_3 nanosheets supported PtPd alloy in selective hydrogenation of naphthalene. *Ind. Eng. Chem. Res.* **2026**, *65*, 6433-43. DOI
169. de, Paula. N. F. L.; Mesa, H. M.; Ortigosa, J. M.; et al. Enhancing hydrocracking catalyst performance and lifetime through surfactant-templated mesoporosity in Pt/HUSY zeolites. *Energy. Fuels.* **2026**, *40*, 730-41. DOI
170. Jin, Y.; Sun, X.; Zhong, H.; et al. Boosting hydrogen spillover with carbon modification: a path to high-performance Cu-ZnO-ZrO_2 catalyst for CO_2 hydrogenation to methanol. *Appl. Catal. B. Environ. Energy.* **2026**, *382*, 125980. DOI
171. Bai, K.; Huang, J.; Tian, M.; Han, C.; Huang, W. Cerium doped Co/AC catalysts for higher alcohols synthesis from syngas. *Mol. Catal.* **2023**, *546*, 113270. DOI
172. Porosoff, M. D.; Chen, J. G. Trends in the catalytic reduction of CO_2 by hydrogen over supported monometallic and bimetallic catalysts. *J. Catal.* **2013**, *301*, 30-7. DOI

173. Zhong, B.; Liang, Z.; Huang, J.; Ye, Y.; Liu, Y.; Wang, T. Effect of CeO_2 morphology in catalytic performance via methanol oxidative steam reforming for hydrogen production. *Ind. Eng. Chem. Res.* **2024**, *63*, 6521-33. DOI
174. Oh, R.; Huang, X.; Hayward, J.; et al. Insights into CeO_2 particle size dependent selectivity control for CO_2 hydrogenation using Co/CeO_2 catalysts. *ACS. Catal.* **2024**, *14*, 897-906. DOI
175. Mei, D.; Sun, M.; Liu, S.; Zhang, P.; Fang, Z.; Tu, X. Plasma-enabled catalytic dry reforming of CH_4 into syngas, hydrocarbons and oxygenates: insight into the active metals of γ-Al_2O_3 supported catalysts. *J. CO2. Util.* **2023**, *67*, 102307. DOI
176. Ye, J.; Li, G.; Ye, F.; Xie, W.; Chen, Q. Engineering oxygen vacancies in non-noble Cu_xFe_1/ZrO_2 catalysts for synthesis of *N*,*N'*-diphenylurea from CO_2 and aniline. *Ind. Eng. Chem. Res.* **2026**, *65*, 8166-81. DOI
177. Li, Y.; Zhao, Z.; Jiang, M.; et al. Selective conversion of syngas to C_{4+} long-chain alcohols. *Nat. Commun.* **2026**, 17. DOI PubMed PMC
178. Qin, T.; Lin, T.; Qi, X.; et al. Tuning chemical environment and synergistic relay reaction to promote higher alcohols synthesis via syngas conversion. *Appl. Catal. B. Environ.* **2021**, *285*, 119840. DOI
179. Dang, Y.; Han, Q.; Wang, R.; Wei, Z.; Wang, M.; Qin, B. Atomic perspective elucidates mixed alcohol synthesis from syngas on bilayered (K)/MoS_2 catalysts. *RSC. Adv.* **2025**, *16*, 1-10. DOI
180. Guo, S.; Li, Z.; Yin, R.; et al. Oxygen vacancy over $CoMnO_x$ catalysts boosts selective ethanol production in the higher alcohol synthesis from syngas. *ACS. Catal.* **2023**, *13*, 14404-14. DOI
181. Osman, M. E.; Maximov, V. V.; Dipheko, T. D.; et al. Synthesis of higher alcohols from syngas over a K-modified CoMoS catalyst supported on novel powder and fiber commercial activated carbons. *ACS. Omega.* **2022**, *7*, 21346-56. DOI PubMed PMC
182. Barberis, L.; Versteeg, C. I.; Meeldijk, J. D.; Stewart, J. A.; Vandegehuchte, B. D.; de Jongh, P. E. K and Na promotion enables high-pressure low-temperature reverse water gas shift over copper-based catalysts. *ACS. Catal.* **2024**, *14*, 9188-97. DOI
183. Lonergan, W. W.; Vlachos, D. G.; Chen, J. G. Correlating extent of Pt-Ni bond formation with low-temperature hydrogenation of benzene and 1,3-butadiene over supported Pt/Ni bimetallic catalysts. *J. Catal.* **2010**, *271*, 239-50. DOI
184. Lonergan, W. W.; Xing, X.; Zheng, R.; Qi, S.; Huang, B.; Chen, J. G. Low-temperature 1,3-butadiene hydrogenation over supported Pt/3d/γ-Al_2O_3 bimetallic catalysts. *Catal. Today.* **2011**, *160*, 61-9. DOI
185. Okatsu, H.; Morrill, M. R.; Shou, H.; et al. Supported K/MoS_2 and K/Mo_2C catalysts for higher alcohol synthesis from synthesis gas: impact of molybdenum precursor and metal oxide support on activity and selectivity. *Catal. Lett.* **2014**, *144*, 825-30. DOI
186. Yao, R.; Yu, Y.; Wu, B.; et al. Synergistic Na-S modified Fe-Cu catalysts for efficient CO_2 hydrogenation to higher alcohols. *Chem. Eng. J.* **2025**, *512*, 162498. DOI